Climate Data Record (CDR) Program

Climate Algorithm Theoretical Basis Document (C-ATBD)

AVHRR Radiances - NASA

Calibration of Historical and Future AVHRR and GOES Visible and Near-Infrared Sensors

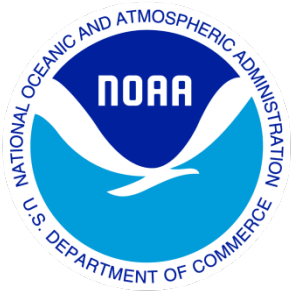

CDR Program Document Number: CDRP-ATBD-0823
Configuration Item Number: 01B-30a
Revision 1/ July 10, 2016

REVISION HISTORY

Rev.	Author	DSR No.	Description	Date
1	D. Doelling & P. Minnis, NASA Langley Research Center	DSR-1048	Baselined Submission to CDR Program	07/10/2016

TABLE of CONTENTS

LIST of FIGURES

LIST of TABLES

1. Introduction

1.1 Purpose

Calibrating old, current, and future satellite imagers in a consistent fashion for climate studies is an outstanding problem that is being addressed by various groups around the globe (Goldberg et al. 2011). The purpose of this document is to describe the algorithm submitted to the NCDC by Patrick Minnis (NASA LaRC) that will be used to create the Solar Channels Calibration FCDR for the NOAA and MetOp POES AVHRRs and the GOES imagers covering a time period of more than 30 years. The actual algorithms are defined by the computer program (code), which accompanies this document. The intent here is to provide a guide to understanding that algorithm, from both a scientific perspective and in order to assist a software engineer or end-user performing an evaluation of the code.

1.2 Definitions

Following is a summary of the symbols used to define the algorithms.

Calibration coefficient parameters:

$\Delta\lambda$ = band width (μm) *(1.01)*

δ = *directional reflectance model* ($Wm^{-2}sr^{-1}\mu m^{-1}$) *(1.02)*

λ = wavelength (μm)) *(1.03)*

μ_0 = cosine of the solar zenith angle *(1.04)*

ρ = reflectance *(1.05)*

σ = standard deviation of the standard error *(1.06)*

χ = BRDF *(1.07)*

g = gain ($Wm^{-2}sr^{-1}\mu m^{-1}cnt^{-1}$) *(1.08)*

BTD = BT difference (K) between 10.7 and 12.0-μm channels *(1.09)*

C = earth view count *(1.10)*

C_{dual} = dual-gain count *(1.11)*

C_{high} = high-gain count for dual-gain calibration *(1.12)*

C_o = space view count or offset *(1.13)*

C_{single} = single-gain equivalent count for dual-gain calibration *(1.14)*

CW = central wavelength (μm) *(1.15)*

DERM = DERM ($Wm^{-2}sr^{-1}\mu m^{-1}$) *(1.16)*

d = relative Earth-Sun distance *(1.17)*

t = day since satellite launch *(1.18)*

E_o = band solar constant ($Wm^{-2}\mu m^{-1}$) *(1.19)*

g_o, Δg_1, Δg_2 = calibration gain coefficients *(1.20)*

[illegible] low-gain calibration line intercept *(1.21)*

L = spectral radiance ($Wm^{-2}sr^{-1}\mu m^{-1}$) *(1.22)*

L_{DCC_norm} = spectral radiance ($Wm^{-2}sr^{-1}\mu m^{-1}$) *(1.23)*

L_{pseudo} = spectral radiance ($Wm^{-2}sr^{-1}\mu m^{-1}$) *(1.24)*

L_{ref} = reference spectral radiance ($Wm^{-2}sr^{-1}\mu m^{-1}$) *(1.25)*

L_{tar} = target spectral radiance ($Wm^{-2}sr^{-1}\mu m^{-1}$) *(1.26)*

M = incoming band solar radiance ($Wm^{-2}sr^{-1}$) *(1.27)*

R = relative spectral response *(1.28)*

Slope = low-gain calibration line slope ($Wm^{-2}sr^{-1}\mu m^{-1}cnt^{-1}$) *(1.29)*

Split = intersection count for dual gain lines *(1.30)*

w = uncertainty weight = $1/\sigma^2$ *(1.31)*

U = uncertainty *(1.32)*

1.3 Document Maintenance

This document is under version control. Any updates to the FCDR will be accompanied by further documentation. There should not be an update to the documentation of future launched GOES and AVHRRs utilize the same algorithms in the ATBD, although, there will be updates to the calibration coefficients table. If there are algorithm updates to the calibration methodologies, then the ATBD will be updated.

2. Observing Systems Overview

2.1 Products Generated

The FCDR products generated are the GOES and AVHRR VIS, VEG and NIR calibration coefficients to convert the sensor pixel-level digital counts to radiances. These in turn are used to retrieve the TCDR consistent long-term cloud and clear-sky properties from all historical and current AVHRR sensors available at the NOAA CLASS archive (Minnis, 2014). Similar analyses could be applied to the historical GOES series. The calibration coefficients are derived from a multiple calibration methods that are uniformly applied to all sensors and tied to a common calibration reference in order to mitigate any spurious drifts in the retrieved cloud properties due to sensor calibration degradation and multiple sensor records. The application of the calibration coefficients is described in section 3.4.1. The calibration coefficients and associated uncertainties are disseminated in a simple ASCII tables and described in section 3.4.7.

2.2 Instrument Characteristics

2.2.1 AVHRR Instrument Characteristics

The Advanced Very High Resolution Radiometer (AVHRR) has flown on TIROS, NOAA, and Metop platforms for over 30 years in both morning and afternoon sun-synchronous low-Earth polar orbits. Typically, the orbits precessed after launch, eventually culminating in a terminator orbit, after which the platform was replaced by another satellite at its nominal equatorial crossing time. Three versions of the AVHRR were built. All versions employed visible (0.65 μm), vegetation (0.86 μm), shortwave infrared (3.75 μm), and infrared window (10.7 μm) channels. The earlier morning orbiters typically lacked a split window infrared (12.0 μm) channel, which is included on all afternoon orbiters and all AVHRR/3 instruments. The AVHRR/3 version also added the near-infrared 1.6-μm channel, which replaces the 3.75-μm channel during the day on some platforms. The nominal pixel resolution for all channels is 1 km and is available in the HRPT or LAC format. Complete spatial coverage is only available in the GAC format, which has a pixel resolution of 4 km. The VIS channel digital count resolution is 10 bit for all channels. Except for AVHRR/3, the digital counts are proportional to radiance. For AVHRR/3, a non-linear dual gain approach is taken, where greater count resolution is viewed under clear-sky conditions or low-sun conditions, and reduced count resolution under cloudy and snow-covered conditions. The calibration coefficient table will provide a list of all the NOAA and MetOp satellites, valid duration of the coefficients, and channels available. A list of the NOAA ad MetOp satellites is also provided by Minnis (2014). Detailed description of the AVHRR instruments can be found in the NOAA POD and NOAA KLM users guides (http://www.ncdc.noaa.gov/oa/pod-guide/ncdc/docs/klm/index.htm), (http://www.ncdc.noaa.gov/oa/pod-guide/ncdc/docs/podug/index.htm).

2.2.2 GOES Imager Characteristics

The GOES record began in 1978 with GOES-1 and continues to the present (December 2013) with GOES-13 and GOES-15 operating at the nominal east and west positions. The GOES reside in geo-synchronous orbits. Typically, two GOES are in operation simultaneously, one located at 135°W (GOES-West) and the other at 75°W (GOES-East). Occasionally, only one is in operation and can be positioned anywhere in between. To fill a gap coverage over the western Pacific, GOES-9 was moved to 160°E during 2003 to 2005. The following web site can provide specific equatorial locations and temporal coverage of the GOES satellites: http://www.ssec.wisc.edu/datacenter/ (select geostationary satellite image browse and calendar). Two versions of GOES instruments have been deployed. The original, pre-GOES-8 imager is the VISSR, which uses the spin of the satellite to scan east to west while stepping the mirror vertically to achieve north-south scan lines. It has one VIS channel and two infrared channels. The VISSR VIS pixels have a nominal visible pixel resolution of 0.9 km with an oversampling of 0.7 km. The VISSR has a 6-bit digital count resolution, where the squared count resolution is proportional to radiance. Clark (1983) provides details of the GOES 1-7 systems. The early GOES VIS spectral response functions (SRFs) were quite broad. The width was reduced somewhat for later GOES imagers. The post-1994 GOES-8 through GOES-15 instruments onboard 3-axis stabilized satellites have one visible channel (0.65 μm) and four infrared channels with a nominal visible pixel resolution of 1 km with slight oversampling in the East-West dimension to increase the pixel resolution to 0.6-km. The sensor dynamic resolution is 10 bit counts. Further information can be found here (http://goes.gsfc.nasa.gov/text/goestechnotes.html). Lower spatial resolutions are usually obtained by subsampling.

2.2.3 MODIS Instrument Characteristics

The absolute reference source for the calibration of the GOES and AVHRR data is provided by Collection 6 radiances from MODIS on Terra and Aqua. Terra and Aqua are in well-maintained sun-synchronous orbits with 1030 and 1330 local equatorial crossing times, respectively. The cross-track scanning MODIS consists of 36 channels having spatial resolutions between 250 m and 1 km. MODIS channels 1 (VIS), 2 (VEG), and 6 (NIR) are used as the references for this calibration effort. Specifically, the Aqua MODIS, operating since June 2002, is used for the VIS and VEG channel calibrations, while the Terra MODIS, operating since January 2000, is the reference for the NIR channel. Additionally, by normalizing the Terra channels 1 and 2 to their respective Aqua counterparts (e.g., Minnis et al. 2008, Doelling et al. 2015), the Terra data can substitute for Aqua as calibration references for the VIS and VEG channels. Radiances taken at the 1-km resolution are used here; they are obtained via averaging of the higher resolution pixels. More information related to the MODIS instrument can be found in Barnes et al. (1998) and at the following URL: http://modis.gsfc.nasa.gov/about/.

Examples of the SRFs of the target (i.e., AVHRR and GOES) and reference (MODIS) channels are plotted in Figure 1. The MODIS reference channels are narrower than the target channels in all cases, but, except for GOES-5 in Figure 1a, are well centered within the target channel responses. Calibrating the target channels against the reference

channels requires normalization of the reference radiances to the target channel SRFs. This is accomplished using spectral band adjustment factors (SBAF) discussed in section 3.2.4. Further SRF comparisons can be performed using the NASA-Langley SRF web tool (http://cloudsgate2.larc.nasa.gov/cgi-bin/site/showdoc?docid=194)

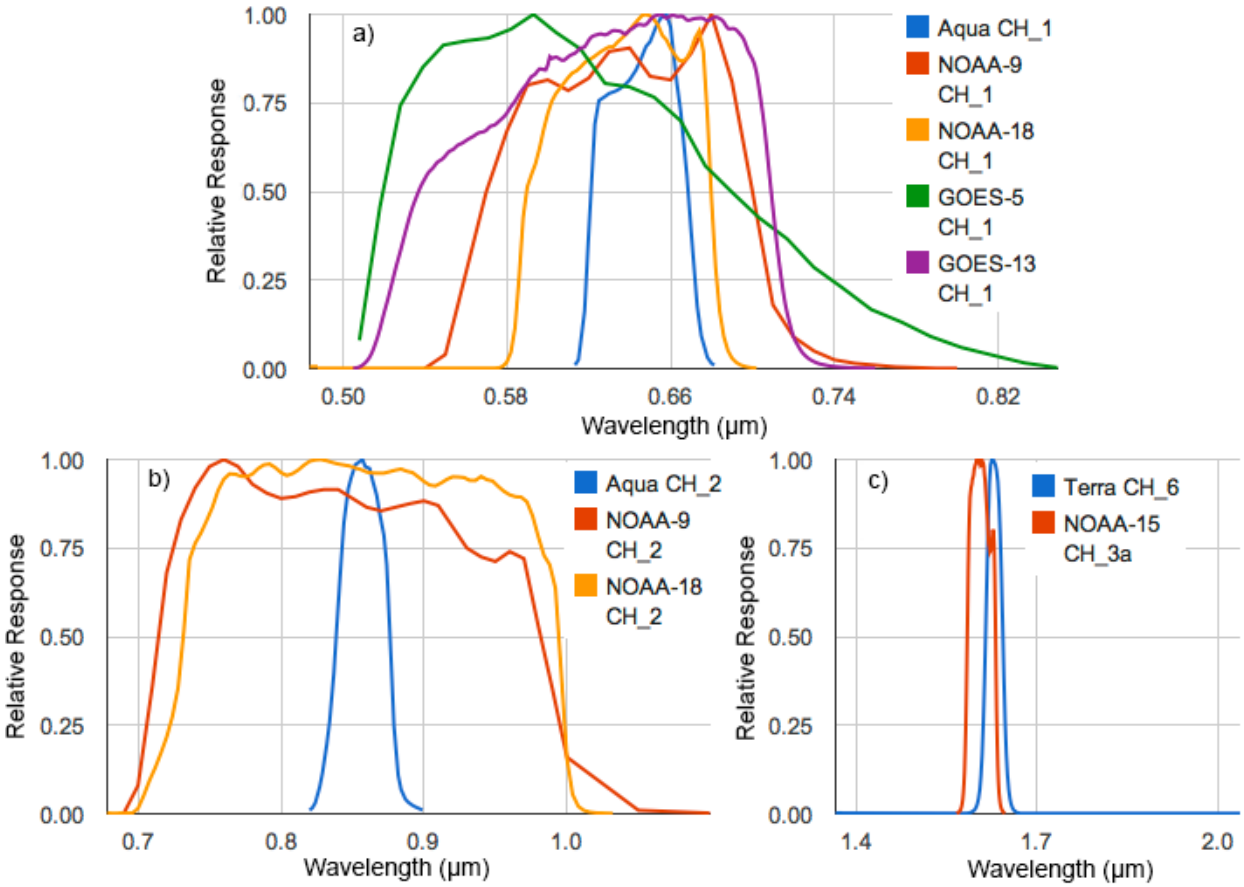

Figure 1: Spectral response functions (SRFs) of relevant channels on several satellite imagers. (a) VIS, (b) VEG, and (c) NIR.

3. Algorithm Description

3.1 Algorithm Overview

The AVHRR and GOES FCDR calibration coefficients are derived using a multiple calibration method approach that is designed to be uniformly applied across all individual satellite visible imagers to produce climate quality visible radiances. The results should permit the consistent retrieval of cloud properties over the entire 30-year record. If more than one result is available, the individual calibration technique results are combined to derive a single set of calibration coefficients. This merging is designed to give the greatest weight to the particular calibration technique having the least uncertainty for a particular satellite. The uncertainty depends on viewing domain, SRFs, and other orbit and imager characteristics. The calibration coefficients are referenced to the MODIS calibration reference. Each of the techniques provides an independent path for transferring the reference calibration.

3.2 Processing Outline

AVHRR calibration coefficients are derived using up to four different calibration methods. Each method transfers the reference calibration of Aqua MODIS channels 1 and 2 with AVHRR VIS and VEG channels, respectively. The first three methods are based on desert, polar ice and DCC invariant targets. The last method is the Aqua MODIS and AVHRR SNO method, which directly transfers the MODIS reference calibration by matching MODIS and AVHRR coincident collocated and co-angled radiance pairs. This method is only available during the Aqua time period (2000 – present).

In order to calibrate AVHRR channels uniformly over the entire AVHRR record, desert, polar ice and DCC invariant targets are used to transfer the MODIS calibration. Because the reflectances of these scenes depend on the viewing and illumination angles, it is necessary to account for these dependencies because the MODIS observations are constrained to particular ranges in SZA over a given location. To account for difference, it is necessary to account for the reflectance anisotropy by (1) minimizing the VZA and RAA effects by using only near-nadir observations and (2) modeling it as a function of SZA using a directional model or DM. The Aqua MODIS observations cannot be used directly to construct the DM due to SZA sampling limitations. Therefore, the NOAA-16 AVHRR reference radiances are used to characterize the reflectance as a function of SZA over the invariant targets, where the NOAA-16 reference calibration is based on the SNO method. The NOAA-16 satellite was launched into an afternoon orbit, then drifted into a terminator orbit, and then into a morning orbit between 2001 and 2013. The Aqua-MODIS DCC reference calibration transfer does not require coincident observations but assumes that the AVHRR and Aqua-MODIS DCC mean radiance is constant over 30 years during the local MODIS overpass time periods.

The three invariant target calibrations are then combined into a single set of coefficients based on the uncertainty of each calibration. The combined calibration is then evaluated against the SNO calibration method. This calibration strategy is used for both the

AVHHR VIS and VEG channels. Because the Aqua-MODIS NIR channel has many inoperable detectors and cannot be used to calibrate the AVHRR 3a band, the Terra-MODIS channel 6 is used instead as the reference calibration. Since the AVHRR NIR channel is only available during the Terra-MODIS time period, no invariant target calibration methods are necessary. The AVHRR calibration strategy is summarized in Table 1.

The GOES calibration methods are similar to that used for AVHRR, except that the polar ice invariant target is not used, since the GOES imagers cannot see it. Table 2 summarizes the GOES calibration strategy. The direct transfer of the Aqua MODIS reference calibration is the primary method. The method is not limited to SNO events, but relies on off-nadir ray-matched events to increase sampling. The GOES desert and DCC methods are not as robust as the AVHRR desert and DCC methods, since the best desert targets are not located over the GOES domain, and there is a limited amount of DCC over the GOES domain. Most of the tropical DCC exists over the tropical western pacific. The GOES desert calibration method relies on a specific DERM that is unique to each sub-satellite point, since the daily viewing geometry is replicated annually with the same scan schedule. The GOES satellites have been at placed at 5 distinct locations over the last 30 years and each position requires a reference GOES satellite to derive the DERM. The DERM reference calibration is based on the GOES/MODIS ray-matched calibration. The GOES DCC reference radiance is equivalent to the MODIS DCC radiance over the GOES domain.

Table 1: AVHRR calibration methods employed by each of the NOAA and Metop satellites.

AVHRR calibration methods, 0.65µm and 0.86µm channels				
Satellites	Aqua/SNO	Deserts	Polar Ice	DCC
NOAA-15/16/17/18/19 Metop-A/B	Validation of Primary	Primary Combined Approach		
NOAA-6/7/8/9/10/11/12/14	N/A			
AVHRR calibration methods, 1.6µm				
Satellites	Terra/SNO	Deserts	Polar Ice	DCC
NOAA-16, 17, Metop-A	Primary	Not Applied		

Table 2: Calibration methods employed by each of the GOES satellites.

GOES calibration methods, visible channel			
Satellites	Ray-match	Deserts	DCC
GOES-10/11/12/13/14/15 GOES-9 (160°E)	Primary	Validation of GEO reference models with Primary Calibration	
GOES-1/2/3/4/5/6/7/8 GOES-9 (135°W)	N/A	Primary Combined Approach	

Each technique is applied independently and is outlined in separate sub-sections below. All methods require systematic processing through all available files for the entire data record. If the method relies on a specific geographical domain, then ground-track prediction software based on the NORAD TLEs or sub-setting options at NOAA-CLASS is used to filter by location. This reduces the processing time. In a similar fashion, GOES image times are predicted prior to processing and only the region of interest is analyzed from the fully scanned image. McIDAS software (Lazzara et al. 1999) is used to process the GOES images, which are in ingested in area file format. The processing procedure of the pixel data is the same whether the method is used as the primary, validation or reference calibration.

3.2.1 Clear Invariant Target: AVHRR Desert and Polar Ice Calibration

The invariant target method is based on the assumption that the average reflectance from a particular clear scene for a given set of viewing and illumination conditions does not vary significantly from year to year and has a predictable seasonal cycle. Thus, for a given time of year and viewing and illumination angles, the target and reference satellites should measure the same reflectances after normalization of the reference satellite radiance to the target satellite SRF using the appropriate SBAF. Use of a bright scene is important to ensure a large dynamic range and reduce the uncertainty in the slope. Barren deserts and ice caps are optimal for this method. The AVHRR desert and polar invariant target ROIs are listed in Table 3.

For each ROI, the counts from AVHRR GAC pixels having VZA < 10° are averaged and the spatial homogeneity is computed. If the spatial homogeneity is less than the clear-sky threshold, the average value is utilized to compute an instantaneous gain. The spatial homogeneity threshold is specific for each satellite sensor over the ROI and is consistently the lowest instantaneous spatial standard deviation. The GOES calibration approach only uses data taken over the Sonoran desert site for specific UTC image times near local noon, as listed in Table 4. The reference and target GOES both use the same UTC image time to ensure angular matches for each Julian day. Again, an instantaneous spatial standard deviation is used to determine the clear-sky days for applying the DERM. Spatial homogeneity is computed specifically for each sensor.

The individual steps in the GOES and AVHRR desert and AVHRR polar ice invariant target calibration processes are summarized in Figure 2. Once the instantaneous observations have been processed, they are averaged for each month. The corresponding

AVHRR reference DM-predicted radiances are also averaged monthly. Then, the monthly gain is computed and the temporal trend is determined to provide the calibration coefficients.

Table 3: The AVHRR desert and polar ice ROIs

AVHRR and GOES desert and polar ice sites							
Site	Libya-4	Libya-1	Niger-1	Arabia-1	Dome-C	Greenland	Sonoran
Sensor	AVHRR	AVHRR	AVHRR	AVHRR	AVHRR	AVHRR	GOES
North	28.80	24.67	19.45	19.13	-74.80	73.00	32.10
South	28.30	24.17	18.95	18.63	-75.40	72.00	31.90
East	23.65	13.60	10.05	47.01	123.7	-39.00	-114.4
West	23.15	13.10	9.55	46.51	123.1	-40.00	-114.6
Size	0.5°x0.5°	0.5°x0.5°	0.5°x0.5°	0.5°x0.5°	0.6°x0.6°	1.0°x1.0°	0.2°x0.2°

Table 4: GOES sensors as a function of sub-satellite point and their associated desert reference sensors.

GOES sub-satellite positions					
Positions	GOES-West	GOES-Prime	GOES-East	South American	East Pacific
longitude	135°W	105°W	75°W	60°E	160°E
Noon image					N/A
Desert Reference	GOES-11	GOES-13	GOES-12	GOES-12	N/A
Satellites	GOES-1,3,4,6,7 ,9,10,11,15	GOES-6,7,13	GOES-2,5,7,8, 12,13	GOES-10	GOES-1,9

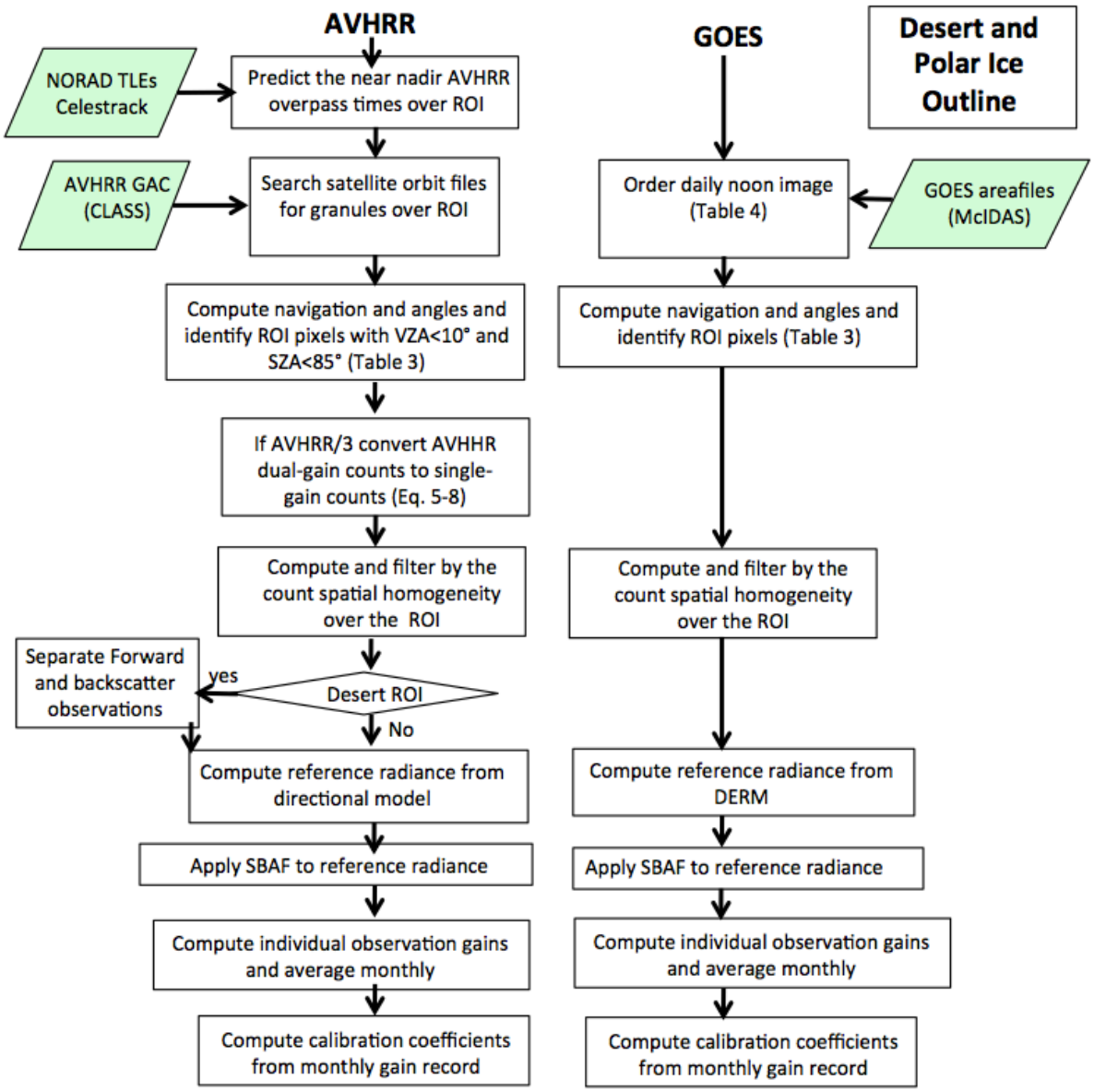

Figure 2: Desert and polar ice calibration method flowchart

3.2.2 Cloudy Invariant Target: AVHRR and GOES DCC Calibration

The DCC method relies on the assumption that the cores of deep convective clouds produce a predictable average reflectance and distribution of reflectances for a given SZA, viewing conditions, and domain. Thus, the challenge is to identify DCC cores within a particular SZA range for a given area. Also, it is important to ensure that the more isotropic part of the angular geometry is considered. To meet the angular requirements, SZA and VZA restrictions are implemented. To increase processing speed, only DCC pixels over the equatorial zone are used. For GOES, a simple UTC image time range is sufficient to find the desired SZA ranges for a domain near the sub-satellite point. DCC cores are assumed to be cold, bright, and uniform in reflectance. Thus, an IRW BT threshold is employed to identify the coldest pixels, while spatial homogeneity tests based on the standard deviations of the VIS reflectance and IRW BT are used to ensure uniformity of the cloud top. The DCC pixels are identified using Table 5.

Table 5: AVHRR and GOES DCC filters.

AVHRR and GOES DCC filters		
Parameter	AVHRR thresholds	GEO thresholds
Latitude extent	±20° N/S all surface types	±20° N/S all surface types
Longitude extent	Global	±20° E/W of GEO sub-satellite point
Solar Zenith Angle	<75°	<40°
View Zenith Angle	<40°	<40°
11µm temperature	BT<205°K	BT<205°K
11µm homogeneity	sBT<1°K	sBT<1°K
Visible homogeneity	sVIS<3%	sVIS<3%
Local Time	N/A	12pm<image time<3PM

After the DCC pixels have been identified, it is necessary to normalize reflectance to the reference SZA, VZA, and RAA. This accomplished by applying the BRDF model (Hu et al. 2004) to the observed DCC radiances to obtain radiances normalized to a nadir view. Monthly frequency histograms are then calculated to determine the mode or mean DCC normalized radiance. The DCC SBAF for the target satellite is then applied to the MODIS reference DCC normalized radiances. As long the MODIS radiances that encompass the same domain and time as either AVHRR or GOES they can be used to predict the monthly DCC gain. Trend analysis is then performed to compute the calibration coefficients. The DCC flowchart is displayed in Figure 3.

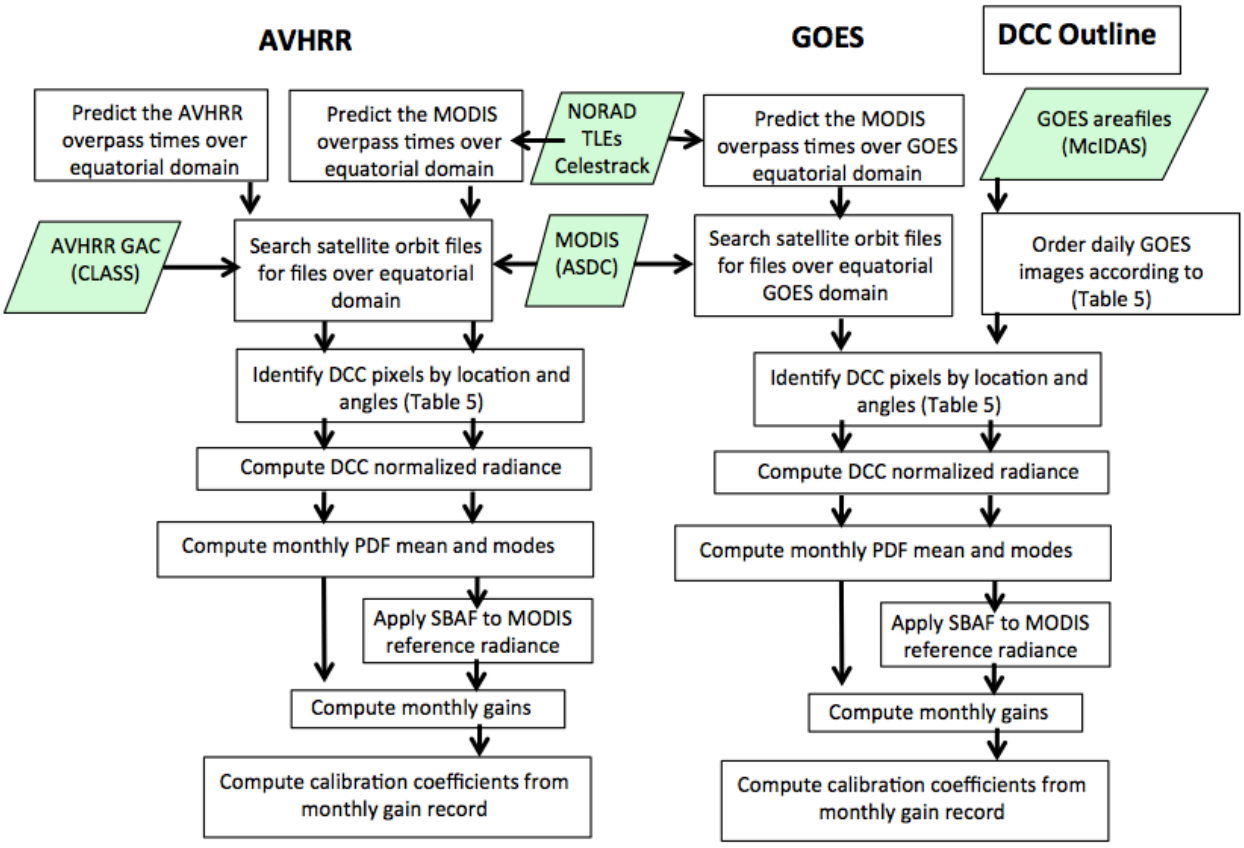

Figure 3: DCC calibration method flowchart.

3.2.3 AVHRR SNO and GOES RM calibration

The SNO and RM techniques rely on the assumption that the reference and target satellites will, on average, measure the same radiances, within a small time window and narrow angular ranges, after normalization of the reference radiance to the target SZA by multiplying by the ratio of the target cos(SZA) to the reference cos(SZA) and for SRF differences using the SBAF . To apply the SNO technique, orbital prediction software based on NORAD TLEs is used to identify the locations where the AVHRR and MODIS orbits intersect within 10 min of each other and when the SZA < 70°. Because the orbit intersection points are used the data from both satellites will be taken from a nadir view. For each location and time, the pixel radiances for each satellite are averaged over a 50-km FOV centered on the orbit intersection and saved along with the associated navigation, because the orbital prediction software does not necessarily provide the same ground track intersect points as the actual data files.

Orbital prediction software is also used to determine the possible number of RM coincident collocated regional radiance pairs. Only MODIS granules that have a significant number of regional radiance pairs are considered for ray matching with GOES to enhance the processing speed. The radiances pairs are only used for data taken over ocean within 15 min of each other and at VZAs and RAAs that differ by less than 10° and 15°, respectively. Furthermore, no sunglint-affected pixels are allowed and the data domain

boundaries must be within ±20° of latitude or longitude of the GOES sub-satellite point. The instantaneous FOV average MODIS radiances are spectrally adjusted for the target sensor using the appropriate SBAF (section 3.2.5). The instantaneous FOV radiance pairs are then linearly regressed to obtain the monthly gain. Trend analysis is then performed to compute the calibration coefficients as a function of time. The SNO/RM flowchart is shown in Figure 4.

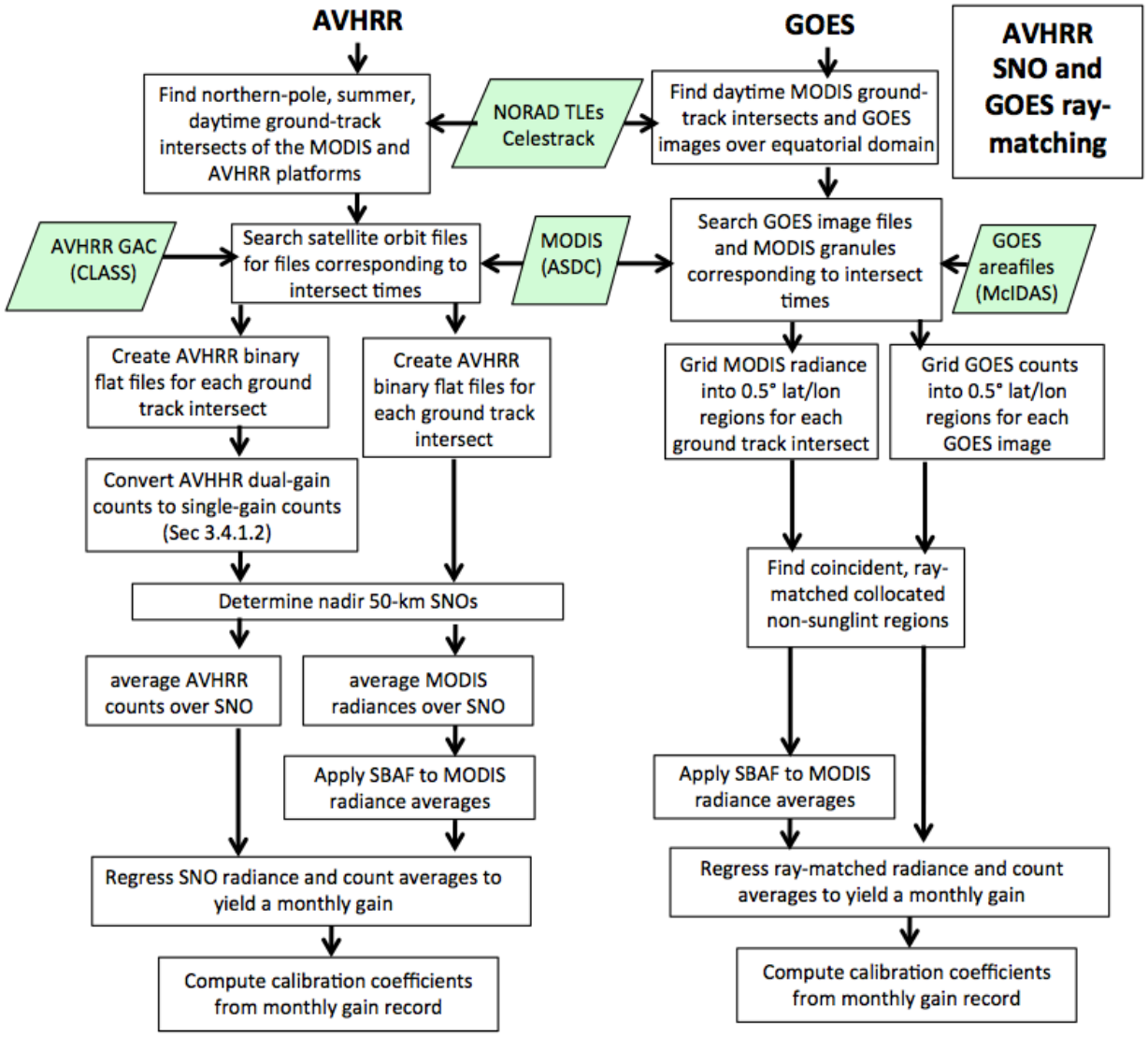

Figure 4: SNO and ray-match calibration method flowchart.

3.2.4 AVHRR and GOES space counts

The desert, polar ice, and DCC invariant target calibration methods require the space view count offset, since they only observe only a narrow dynamic range of Earth view radiances. Ignatov et al. 2005 stated that using a unconstrained intercept when regressing MODIS and AVHRR coincident radiance pairs leads to calibration errors. It was also noted that the space count differs from the pre-launch value and should be recomputed using onboard measurements such as using the dark-side of the Earth count. A space count is

computed from a near-equinox orbit at the beginning and end of each satellite record using a pixel counts with a SZA greater than 110°. If the beginning and end space counts were within 1 count, they were averaged to provide a space count valid over the entire satellite record. If the space count difference was greater than 1, then the space count is computed for all equinox orbits over the record and averaged. The space count is computed for all AVHRR visible channels, since each channel has a unique space count. All calibration methods will use the recomputed space count for consistency.

The GOES 2nd generation beginning with GOES-8 incorporate space clamps that dampen the space count noise to a fixed value, which is well maintained in orbit (Weinreb et al. 1997). The published space count value of 29 is used for the GOES 2nd generation satellites. For the GOES 1st generation satellites the space count is not well maintained. The midnight full disc GMT hour is used to compute the space count from pixels with a SZA greater than 110°. A single space count valid over the entire GOES record is determined. The ISCCP B1U product used multiple data centers to obtain the geostationary imagery. Based on the processing the space count may differ between data centers (Inamdar and Knapp 2015). Most GOES had a stable visible channel space count, except for GOES-7 during 1995.

3.2.5 AVHRR and GOES SBAFs

The SBAF is defined as the ratio of the average radiance for a particular scene type measured by a target satellite to that of reference satellite. The SBAFs for this calibration effort are determined by convolving hyper-spectral SCIAMACHY (Bovensmann et al. 1999) radiances with the SRFs to produce average pseudo radiances for each satellite. These pseudo radiances are then averaged and ratioed to generate the SBAFs.

The SBAF processing flowchart is displayed in Figure 5. The most time consuming part of this process is the sequestering of SCIAMACHY footprints over the invariant target or AVHRR/MODIS SNO or GOES RM domains. This is performed by systematically reading through all of the SCIAMACHY/SSF files. For the surface invariant SBAFs, the SCIAMACHY data must be flagged as clear by the corresponding SSF MODIS cloud amount. The SSF MODIS data are also used to identify DCC scenes to create DCC SBAFs from the SCIAMACHY data. For the SNO or RM domains, all footprints within the domains are used for the SBAFs. All of the footprints over the 10-year SCIAMACHY record are regressed by season to compute the SBAF.

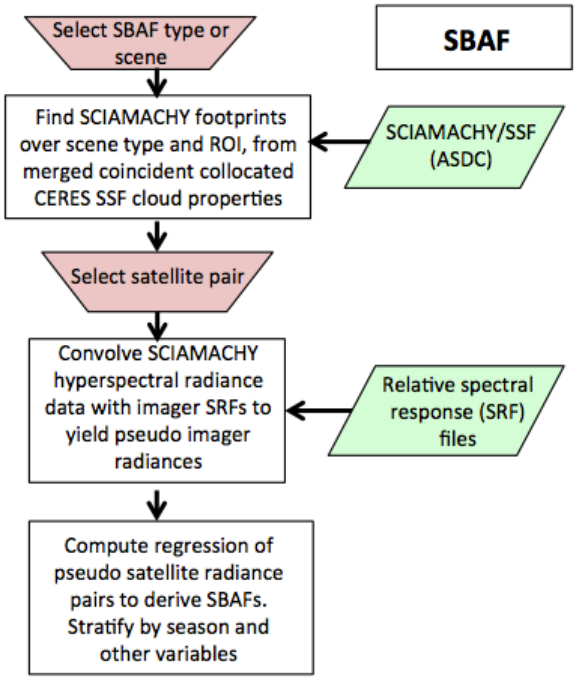

Figure 5: SBAF derivation flowchart.

3.3 Algorithm Input

3.3.1 Primary Sensor Data

Three primary sensor datasets, AVHRR, GOES, and MODIS, are required. The AVHRR GAC Level 1B 10-bit files are read with code developed based on the KLM and POD user guides. (http://www.ncdc.noaa.gov/oa/pod-guide/ncdc/docs/klm/index.htm), (http://www.ncdc.noaa.gov/oa/pod-guide/ncdc/docs/podug/index.htm). The AVHRR data are downloaded from the NOAA CLASS archive (http://www.class.ngdc.noaa.gov/saa/products/search?sub_id=0&datatype_family=AVHRR&submit.x=25&submit.y=5)

The GOES 8 through 15 area files (4-km nominal resolution) are downloaded from the McIDAS server at the Space Science and Engineering Center at the University of Wisconsin, Madison (http://www.ssec.wisc.edu/mcidas/). The GOES area file read code was developed within the McIDAS framework. For GOES 5, 6, 7 ISCCP B1U 3-hourly full disc image files (8-km nominal resolution) are downloaded from the NASA-LaRC ASDC (https://eosweb.larc.nasa.gov).

The Terra and Aqua-MODIS Collection 5 level 1B 5-minute granule data are obtained from the NASA-LaRC ASDC. The CERES project archives a sub-setted MODIS imager dataset at the ASDC. The CERES MODIS data contain a subset of the channel data and are sampled at a 2-km resolution by saving every other line and pixel. The MCST has recently released the Collection 6 MODIS calibrated data, which may not be available for the entire record. In the case where only Collection 5 data are available, the MCST has

provided the Collection 6 calibration coefficients (Aisheng Wu personal communication), which are applied as the Collection 5 data are read.

3.3.2 Ancillary Data

Three ancillary datasets are required. This study employs the Envisat SCIAMACHY Level-1b, Version-7.03 calibrated at-sensor radiances from 2002 through 2010. The SCIAMACHY data volume is ~38 GB per month. The SCIAMACHY 240 km x 30 km footprints are then collocated with coincident CERES SSF 20-km footprints, which include MODIS radainces, and cloud and atmospheric properties. The CERES SSF data are available at the NASA-LaRC ASDC. This combined dataset is maintained by the NASA CLARREO project. The SSF Edition 3 dataset includes the CERES MODIS cloud retrievals based on Minnis et al. (2011) among other parameters.

The NORAD TLEs are downloaded from Celes track web site (http://celestrak.com). TLEs for Aqua, Terra, NOAA, and Metop are updated daily.

The imager normalized SRFs are obtained from various web sites. The AVHRR SRFs are located at the following url:
www.star.nesdis.noaa.gov/smcd/spb/fwu/homepage/AVHRR/spec_resp_func/index.html.
The GOES 8-15 SRFs are obtained at:
www.oso.noaa.gov/goes/goes-calibration/goes-imager-srfs.htm.
The GOES 5-7 are located at the ISCCP SRF page: isccp.giss.nasa.gov/response.html.
The Aqua-MODIS SRFs are obtained via ftp at :
mcst.hbsss-sigma.com/pub/permanent/MCST/FM1_RSR_LUT_07-10-01/.
The Terra-MODIS SRFs are obtained via ftp at :
mcst.hbsss-sigma.com/pub/permanent/MCST/PFM_L1B_LUT_4-30-99/.

3.3.3 Derived Data

Not applicable

3.3.4 Forward Models

Not applicable

3.4 Theoretical Description

3.4.1 Physical and Mathematical Description

The derivation of calibration coefficients is described in this section based on the stepwise processing detailed in section 3.2. First the application of the calibration coefficients is described. The MODIS based invariant target reference models are described as well as the application. The spectral band adjustments are described. Examples of the monthly AVHHR/MODIS SNO or GOES/MODIS ray-matched regression plots are shown.

3.4.1.1 Application of calibration coefficients

The AVHRR and GOES FCDR calibrated radiance L is defined as

$$L = g \bullet (C - C_o), \quad (1a)$$

where C is the visible count, C_o is the space count or offset, g is the gain. The radiance is given in $Wm^{-2}sr^{-1}\mu m^{-1}$. It is important to use the provided C_o when computing the gains, since they were derived using the same value of C_o. For AVHRR/3 sensors, the dual gain count must be converted to a single gain count as described in section 3.4.1.2. For the GOES VISSR, the squared visible counts are proportional to radiance and Equation 1b should be used.

$$L = g \bullet (C^2 - C^2_o). \quad (1b)$$

The gain is expressed as a 2nd order polynomial in time,

$$g = g_o + \Delta g_1 t + \Delta g_2 t^2, \quad (2)$$

since the degradation may not be constant in time. Here t is given in days since launch of the satellite and g_o, Δg_1, and Δg_2 are the gain coefficients. If the sensor degrades linearly in time, then Δg_2 equals zero. If the sensor does not degrade and the calibration is constant in time, then Δg_1 also equals zero. If the reflectance ρ rather than radiance is desired, then it can be computed as

$$\rho = (L \bullet \pi \bullet d^2)/(E_0 \bullet \mu_0), \quad (3)$$

where d is the relative deviation of the Earth-Sun distance from its average value as a function of Julian day, μ_0 is the cosine of the solar zenith angle, and E_0 is the solar constant for the sensor computed by convolving the incoming solar irradiance with the sensor SRF. Since the reference calibrations are based on absolute calibration of the MODIS channels, the official MODIS incoming solar irradiance spectra must be used. E_0 (Wm^{-2}) is also provided as part of the calibration coefficients and is determined as

$$E_0 = [\Sigma M_\lambda \bullet R_\lambda \bullet \Delta_\lambda]/[\Sigma R_\lambda \bullet \Delta_\lambda], \quad (4)$$

where M_λ is the incoming solar radiance in $Wm^{-2}sr^{-1}$, R is the relative spectral response (normalized SRF), and Δ_λ is the bandwidth. The central wavelength is

$$CW_\lambda = [\Sigma R_\lambda \bullet \Delta_\lambda]/[\Sigma \Delta_\lambda]. \quad (5)$$

3.4.1.2 AVHRR Dual-to-Single Gain Count Conversion

The AVHRR/3 (NOAA-15 through 19, Metop) satellites employ dual gain counts C_{dual} – an approach employed in order to increase the sensitivity to low levels of radiance (Heidinger et al. 2002). All calibration procedures of this FCDR are performed using single gain counts, similar to the AVHRR/2 counts. The dual-gain counts are first converted to single-gain counts so as to be linearly proportional to radiance throughout the entire dynamic range of

measurements. Following the methods of Heidinger et al. (2010), C_{dual} is converted to single-gain counts C_{single}. For dual-gain counts below the break point of intersection *Split*,

$$C_{single} = C_o + 0.5 \bullet (C_{dual} - C_o), \quad (6)$$

where the low-gain offset C_o is defined by the NOAA platform-specific nominal count gain $Slope_{nom}$ and offset $Intercept_{nom}$ coefficients as

$$C_o = -(Intercept_{nom}/Slope_{nom}). \quad (7)$$

It is the same as the dark or space count. For dual-gain counts above the *Split*,

$$C_{single} = C_{high} + 1.5 \bullet (C_{dual} - Split) \quad (8)$$

where the high-gain offset C_{high} is defined as follows:

$$C_{high} = C_o + 0.5 \bullet (Split - Intercept_{nom}) \quad (9)$$

Band 3a has a magnification factor of 7 rather than 3 for bands 1 and 3. For channel 3a the 0.5 term in Eq. 6 is replaced with 0.25 and the 1.5 term in Eq. 8 is replaced with 1.75. The $Slope_{nom}$, $Intercept_{nom}$, and *Split* values for each channel are listed in Tables D.1-6 (NOAA-15), D.2-7 (Pre-flight AVHRR, NOAA-16), D.3-4 (NOAA-17), D.4-4 (NOAA-18), D.5-4 (Metop-A), and D.6-4 (NOAA-19) at the web site (http://www.ncdc.noaa.gov/oa/pod-guide/ncdc/docs/klm/html/d/app-d.htm), where they are denoted as the low albedo range *Slope, Intercept*, and *points of intersection,* respectively.

3.4.1.3 Application of Invariant Target Reference Radiance (DM and DERM)

The invariant target reference radiances are used to transfer the MODIS absolute calibration to other satellites. For the AVHRR desert, polar ice, and DCC references, the radiances take the form of a DM, while for GOES the DERM provides the reference radiances as a function of day of the year.

The AVHRR desert and polar ice reference radiances are obtained as follows:

$$L_{ref} = \delta(\mu_o) \bullet d^2, \quad (10a)$$

where δ is the desert or polar ice directional model developed from NOAA-16 reference radiances that were calibrated using the MODIS SNO approach. Equation 10a is also used for the AVHRR DCC DM model (see section 3.4.1.9). A water-vapor correction is necessary for the AVHRR 0.86-μm reference radiance for desert, so an additional term is included:

$$L_{ref} = [\delta(\mu_0) - \Delta L(BTD)] \bullet d^2, \quad (10b)$$

where $\Delta L(BTD)$ is the radiance adjustment based on the difference between the channel-4 (10.8 μm) and channel-5 (12.0 μm) BTs. The DERM reference radiance application is simply

$$L_{ref} = DERM(Julian\ day) \quad (10c)$$

because the Earth-Sun distance correction is embedded in the DERM (see section 3.4.1.8).

3.4.1.4 Spectral Band Adjustment Factor (SBAF) Computation

Normalization of the reference radiance to the target radiance requires correction for the SRF differences. The SBAF approach used here follows Morstad et al. (2011), Doelling et al. (2012), Scarino et al. (2012) and Scarino et al. (2015). The SCIAMACHY hyper-spectral individual footprint (30 km x 240 km) radiances are convolved with an AVHRR, GOES or MODIS SRF in order to derive sensor-equivalent pseudo radiances (L_{pseudo}). The pseudo radiances are computed over the invariant targets and SNO or ray-matching domains used to transfer the Aqua-MODIS calibration reference. Although they are not simultaneously measured with either the AVHRR, GOES or MODIS measurements, they are assumed to capture the same typical clear and cloudy conditions over the invariant targets and matching domains. Since the observed TOA radiances are mainly dependent on water vapor and ozone absorption, the radiance has a seasonal dependence. Thus, the pseudo radiances are computed separately over multiple satellite pairs, domain targets, seasonally, and as a function of precipitable water vapor using the following formulation.

$$L_{pseudo} = [\Sigma\, L_\lambda \bullet R_\lambda \bullet \Delta_\lambda]/[\Sigma\, R_\lambda \bullet \Delta_\lambda] \quad (11)$$

where L_λ is the SCIAMACHY spectral radiance. The summation is performed using all of the SCIAMACHY spectral channels that fall within the bandwidth. The reference radiance is converted to the target radiance by regressing the pseudo radiance pairs. For the DCC and SNO calibration methodologies, a second-order-regression SBAF is used. For the desert and polar ice invariant site methodology, a first-order-regression SBAF, forced through the origin, is used. The SBAF is applied to the reference sensor radiance L_{ref} in order to compute the predicted target sensor radiance L_{tar}:

$$L_{tar} = SBAF_{tar/ref} \bullet L_{ref}, \quad (12)$$

where SBAF represents either the first order or second order regression coefficients.

Figure 6 plots pseudo radiance pairs resulting from using Eq. 11 to convolve the SCIAMACHY spectra with the NOAA-18 AVHRR and Aqua-MODIS band 1 SRFs over the AVHRR/Aqua-MODIS SNO domain defined by the zone between 70° and 80°N. Note there are no seasonal variations in the radiance pairs and the resulting trend is very linear. The resulting force fit slope defines the value of $SBAF_{tar/ref}$ for this case. All spectral band adjustment factors can also be derived using the NASA-Langley SBAF web tool (http://www-angler.larc.nasa.gov/cgi-bin/site/showdoc?docid=223), which computes the pseudo radiances for selected reference and target sensor radiance pairs for a selected Earth target according to method in this section (Scarino et al. 2015).

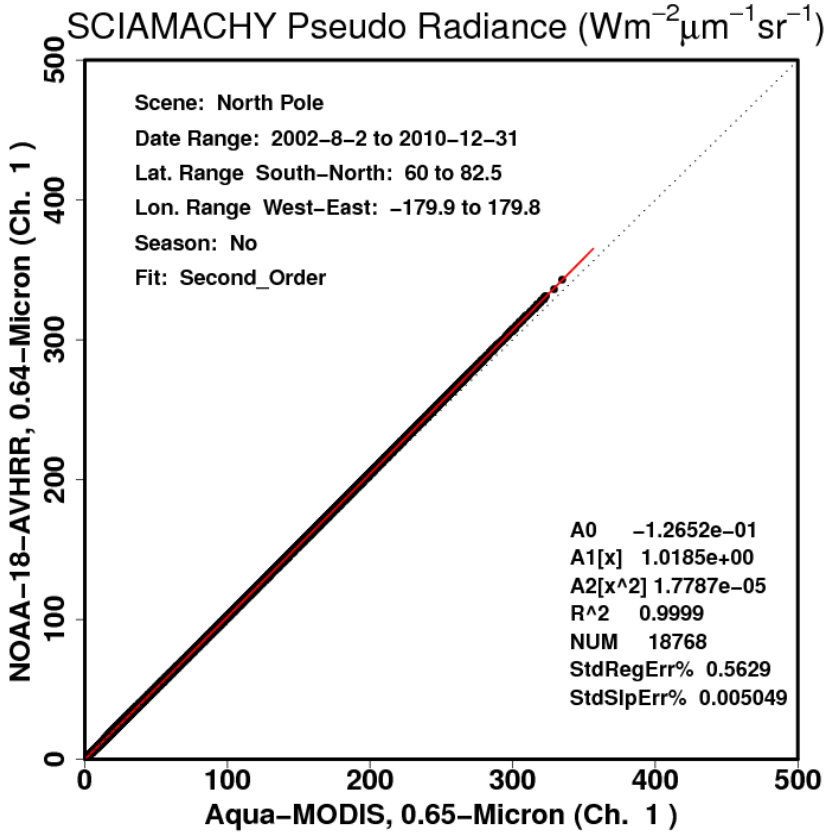

Figure 6: Pseudo NOAA-18 AVHRR and Aqua-MODIS VIS radiance pairs convolved from SCIAMACHY hyper-spectral radiances over the AVHRR/MODIS SNO domain between 70° and 80°N. The associated trend statistics are located in the lower right corner.

3.4.1.5 Computing gain from invariant target reference radiance

In order to compute the gain from the reference radiance, the gain is determined from Eq. 1 by substituting L_{ref} for L and solving. The space count has already been subtracted from the invariant target calibration before application of the model reference radiances (Eq. 10). The temporal trend is then computed using Eq. 2.

3.4.1.6 Combining multiple calibration methods for best estimate gain

For pre-MODIS AVHRR sensors, the final calibration is obtained by combining the desert, polar ice and DCC invariant target calibrations. The desert calibration is the combination of 4 desert sites, each with its own calibration. For polar ice, two sites are used to derive calibration. For historical GOES sensors, only the Sonoran desert is used. Therefore, only the desert and DCC need to be combined for the older GOES imagers.

To combine the multiple invariant target calibrations, the uncertainty of each target is determined by computing the standard error of the trend σ over the sensor record for each approach *i*. Then, a final set of monthly gains g_c is computed by averaging the multiple target monthly gains g_i weighting each by the inverse of the variance σ^2_i. That is,

$$g_c = [\Sigma\, g_i \bullet w_i]/[\Sigma\, w_i], \tag{13}$$

where $w_i = 1/\sigma^2_i$. The time series of g_c is then used to compute the final gain coefficients, which provide the best estimate of the trend.

For example, the NOAA-17 Arabia 1, Libya-1, Libya-4, and Niger-1 VIS trend standard errors are 1.24%, 0.91%, 1.13%, and 1.69%. Figure 7 displays the individual desert gains along with the combined desert and AVHRR/MODIS SNO gains. Note that the combined desert trend standard error is 0.70%, which is lower than any individual desert standard error, validating the multiple desert target approach. In this case, the standard error of the desert and SNO are similar.

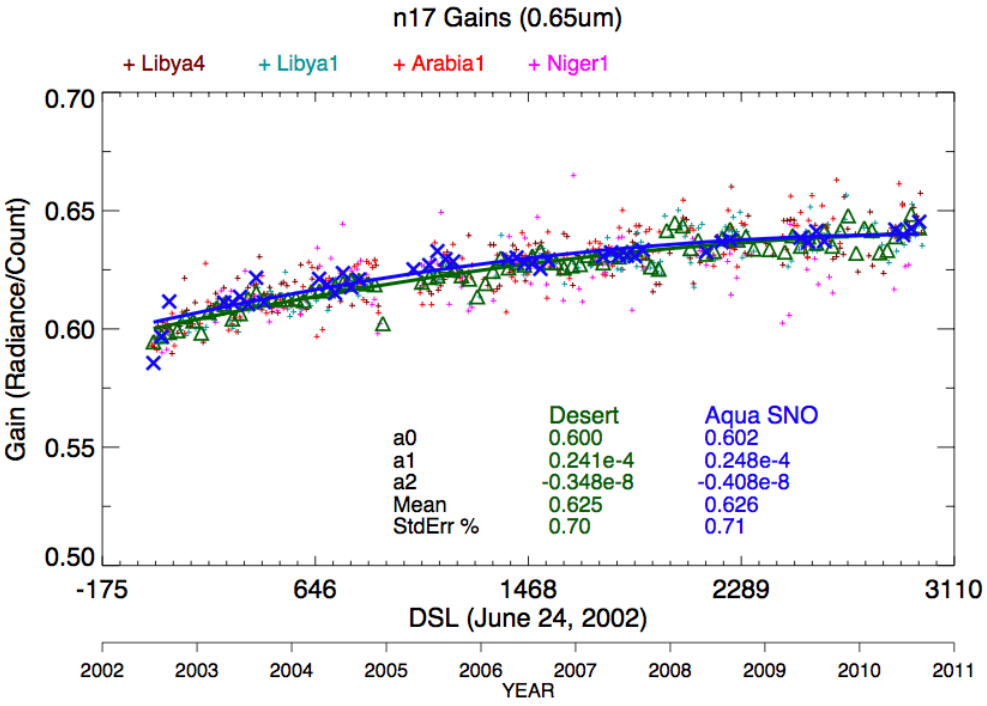

Figure 7: NOAA-17 AVHRR VIS channel monthly desert (green triangles) and AVHRR/Aqua-MODIS SNO calibration gains (blue X) with associated temporal 2nd order trend. Individual desert gains are also plotted.

3.4.1.7 AVHRR desert and polar ice directional models

In order to transfer the Aqua-MODIS VIS absolute calibration to the desert or polar ice invariant target, a DM needed to characterize the SZA dependence of the reflectances. Only near nadir observations (VZA<10°) are utilized to mitigate anisotropic effects. The DM simply quantifies the invariant target radiance variation with μ_0. Unfortunately, due to the degrading AVHRR satellite orbits, the Aqua-MODIS observations cannot be used, since they only observe the invariant targets with a limited SZA range. For example, the sub-tropical deserts are only observed by Aqua or Terra-MODIS at SZA < 60°. Because the NOAA-16 satellite degrades into a terminator orbit during the Aqua-MODIS

record, the AVHRR/MODIS SNO-calibrated NOAA-16 AVHRR radiances are used to construct the DM. This empirical DM can be validated by applying it to any other NOAA platform operating during the MODIS era and then comparing the results with the other platform's SNO calibration. Significant radiance differences as a function of scattering direction were observed over the desert (Bhatt et al. 2013). This was not observed over the polar ice targets. Therefore, over desert, the DM consists of separate forward and backscatter values and over polar ice, only a single DM is needed. Figure 8 displays the observed Libya-4 NOAA-16 AVHRR radiances as a function of μ_0 after removing the Earth-Sun distance factor. The second order regression coefficients are also shown. These coefficients define the DM and the standard error defines the uncertainty. The DM reference radiance is then multiplied by the SBAF to obtain the target sensor radiance. Over deserts, the DM is applied seasonally to remove mean water vapor effects.

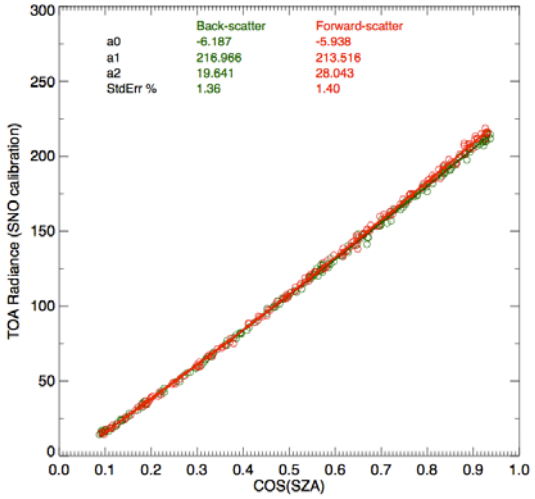

Figure 8: Libya-4 near-nadir TOA NOAA-16 AVHRR VIS radiances stratified by scattering angle as function of μ_0.

As noted earlier, the AVHRR VEG channel radiances are impacted by water vapor. The BTD difference can be used to estimate the precipitable water for the column (Yu et al. 2010). All of the AVHRR instruments have comparable 11 and 12-µm SRFs. Assuming that the temperature difference is consistent for all AVHRR sensors, the observed-minus-predicted reference DM radiance difference as a function based on the BTD was computed for NOAA-16 and is shown in Figure 9 for the Libya-4 desert. The curves are used to supply the values of $\Delta L(BTD)$ in Eq. 10b for Libya-4. The absolute temperature calibration is not necessary, however the relative differences need to be similar for all of the sensors.

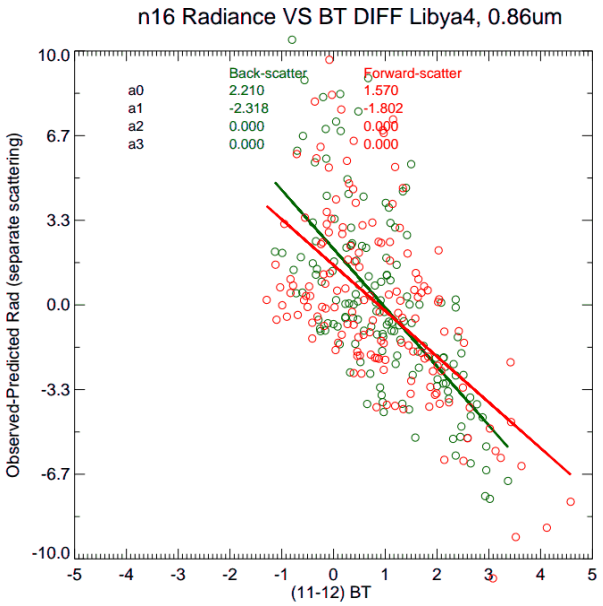

Figure 9: Libya-4 near-nadir TOA NOAA-16 AVHRR observed VEG radiance (W m^{-2} sr^{-1}) minus reference DM difference as function of BTD (K).

3.4.1.8 GOES Sonoran Desert DERM

To transfer the Aqua-MODIS VIS absolute calibration to the Sonoran desert, a Daily Exoatmospheric Radiance Model (DERM) is derived from a reference GOES sensor that has been calibrated using GOES/MODIS RM method (Bhatt et al. 2013). Since the GOES operational imaging schedule is consistent over most of the GOES record, a GOES at a given sub-satellite point will observe the Sonoran desert with the same SZA, VZA and RAA every year for a given Julian day and UTC image time. The DERM consists of all TOA observed radiances at a UTC image time for each Julian day averaged over several years (Figure 10). The standard deviation (Figure 10, right panel) of the annual TOA radiances provides the uncertainty in the error budget. The DERM reference radiance is then multiplied by the SBAF to obtain the target sensor radiance. The DERM is developed for each to account for seasonally varying water vapor and surface effects.

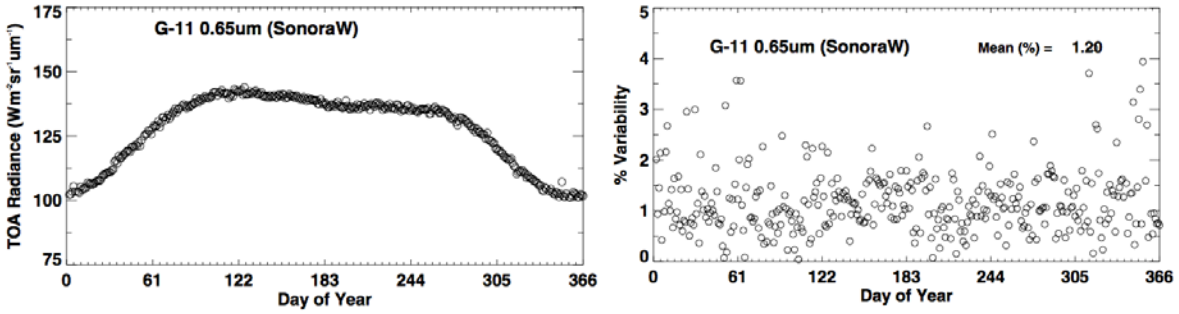

Figure 10: Sonoran GOES-11 19:30GMT DERM (Left Panel) and standard deviation (Right Panel) as a function of Julian day, derived from 5-years of data.

3.4.1.9 DCC calibration method

The DCC calibration method follows the GSICS ATBD (Doelling et al. 2011). The DCC pixels are identified using the filters in Table 5. Although the observed DCC radiances are nearly isotropic, the BRDF χ from Hu et al. (2004) is applied to remove any residual anisotropic effects. The DCC pixel radiances are then normalized to a reference condition at a nadir view:

$$L_{DCC\_norm} = [L \bullet d^2]/[\mu_0 \bullet \chi(SZA,VZA,RAA)]. \quad (14)$$

A PDF of the AVHRR or GOES normalized DCC counts is constructed each month (Figure 11, left panel). The intervals within the PDF are set to ensure that only single modes are obtained, while preserving as much count accuracy as possible. Both the monthly NOAA-18 AVHRR mean and mode VIS counts are monitored over time as in Figure 11 (right panel). Note the smaller standard error about the linear trend for the mode statistic.

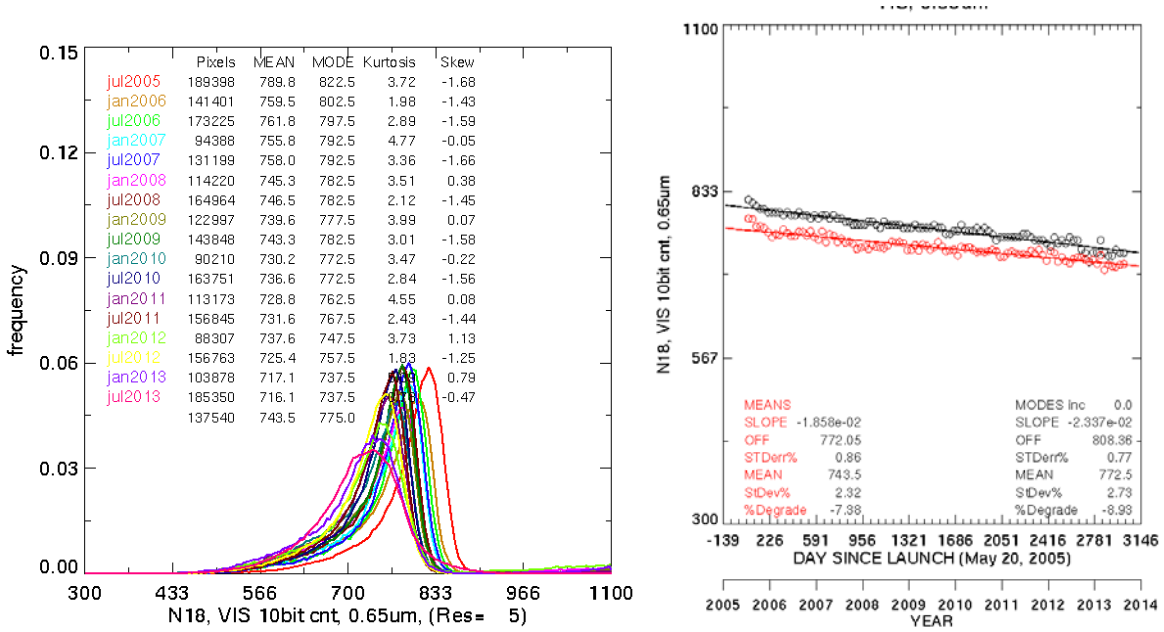

Figure 11: (Left Panel) Monthly PDFS of the NOAA-18 AVHRR VIS BRDF- normalized DCC counts. (Right Panel) Monthly mode and mean DCC counts as a function of time.

For $\lambda < 1$ μm, the mode count provides a smaller temporal trend uncertainty, whereas for $\lambda > 1$ μm, the mean count is better suited for temporal trending (Doelling et al. 2013). For GOES, the monthly mode count is used (Morstad et al. 2011). For the AVHRR VIS channel the PDF mode radiance stable within 40° SZA as shown in Fig. 12. The DM adjustment for 40° <SZA< 60° is necessary because the Hu model does not completely remove the radiance darkening for SZA>40°. The NOAA-16 AVHRR SNO-calibrated radiances are used to compute the DCC PDF mode radiance reference DM. For AVHRR PDF mode radiance DM is used for both VIS and VEG channels.

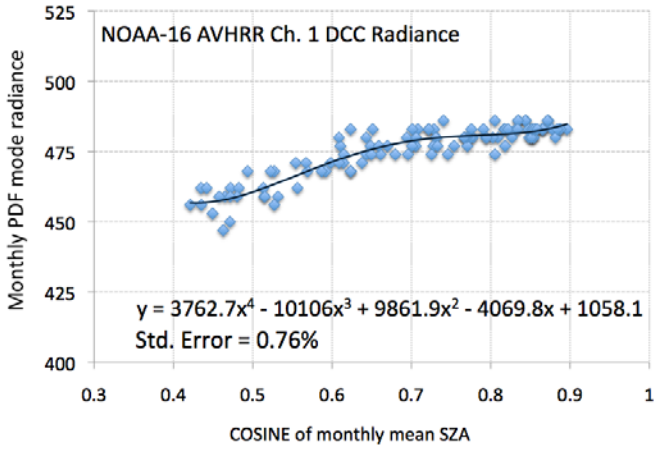

Figure 12: NOAA-16 AVHRR BRDF-normalized DCC radiance as μ_o for both the PDF mode statistic.

3.4.1.10 GOES/MODIS ray matching

The GEO/MODIS RM technique has been in place for many years (Minnis et al. 2002). The approach here follows the GSICS ATBD (Doelling et al. 2011; Morstad et al. 2011). The advantage of GEO/MODIS ray matching is that the full GOES dynamic range can be compared with MODIS nearly every month. Any short-term spurious GOES calibration anomalies can easily be identified, unlike invariant targets, which need years of data to adequately characterize the seasonal variability using the Sonoran desert target. The method for this FCDR is to grid or average the MODIS and the GOES pixel radiances into 0.5° latitude x 0.5° longitude regions. Use of the relatively large areas mitigates any effects from navigational error and cloud movements that occurred due to the time difference. The MODIS radiances are then multiplied by the SBAF to account for the spectral band differences. The spectrally adjusted MODIS radiances are considered the MODIS reference radiances. The SBAF were derived over each of the equatorial GEO domains. The coincident, ray-matched, and collocated regional radiance pairs are then regressed through the GOES space count (Figure 13, left panel). The monthly slopes or gains are then monitored over time to compute the trend coefficients (Figure 13, right panel).

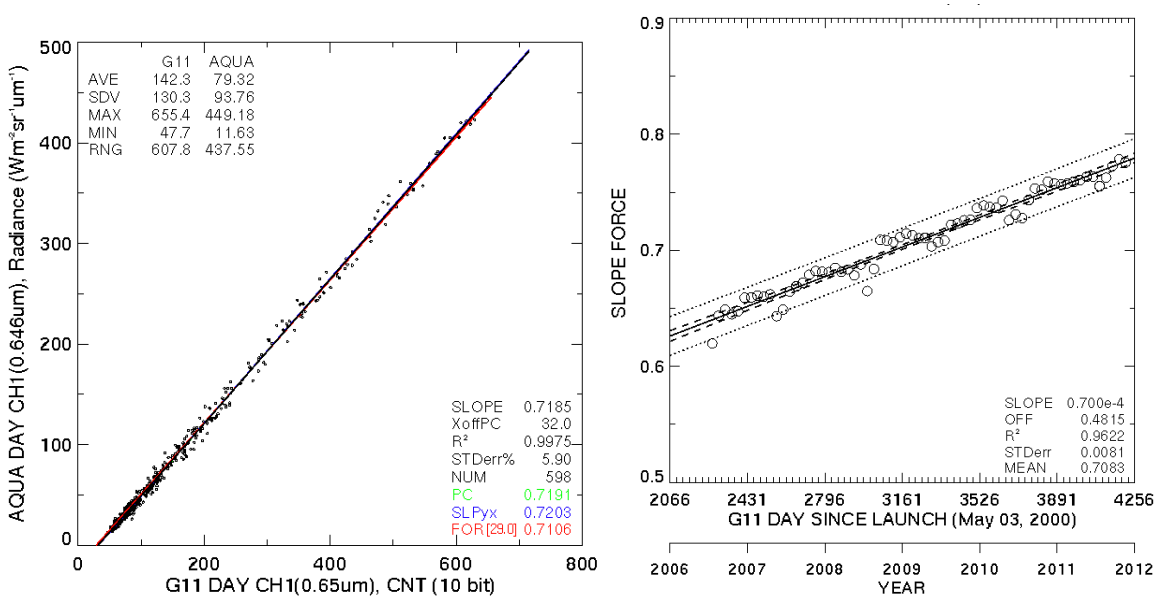

Figure 13: GOES-11/Aqua-MODIS ray-matched radiance pairs for April 2009. Linear regression through the space count shown in red (slope force). Monthly slope or gains and linear temporal trend shown in right panel.

3.4.1.11 AVHRR/MODIS SNO

There have been many studies employing AVHRR/MODIS SNOs to transfer the calibration of MODIS to AVHRR for similar channels (Heidinger et al. 2002, Doelling et al. 2004, Heidinger et al. 2010). The method for this FCDR is to use a 50-km FOV SNO to transfer the MODIS absolute calibration to the AVHRR sensor. The 50-km FOV mitigates the pixel navigational error, and the advective displacement of clouds due to any time difference between the two measurements. If the two sun-synchronous satellite pairs are

in maintained orbits, then the off-nadir FOV can also be utilized, such as Terra and Aqua-MODIS (Minnis et al. 2008, Doelling et al. 2013). The left panel of Figure 14 shows the NOAA-18/Aqua-MODIS 50-km radiance pairs for both nadir-only and off-nadir FOVs for June 2006. During this month the NOAA-18 orbit did not degrade and the SNOs were near noon. The linear regression through the NOAA-18 space count is nearly identical for both nadir-only and off-nadir FOVs. The advantage of the off-nadir FOVs is the increased dynamic range and sampling. However, after the NOAA-18 degrades, the nadir-only and off-nadir monthly slopes diverge after 2011 (Figure 14, right panel). For this study, the nadir-only SNO slopes are utilized. For quality control the nadir-only and off-nadir slopes are compared at the beginning of the NOAA records for consistency.

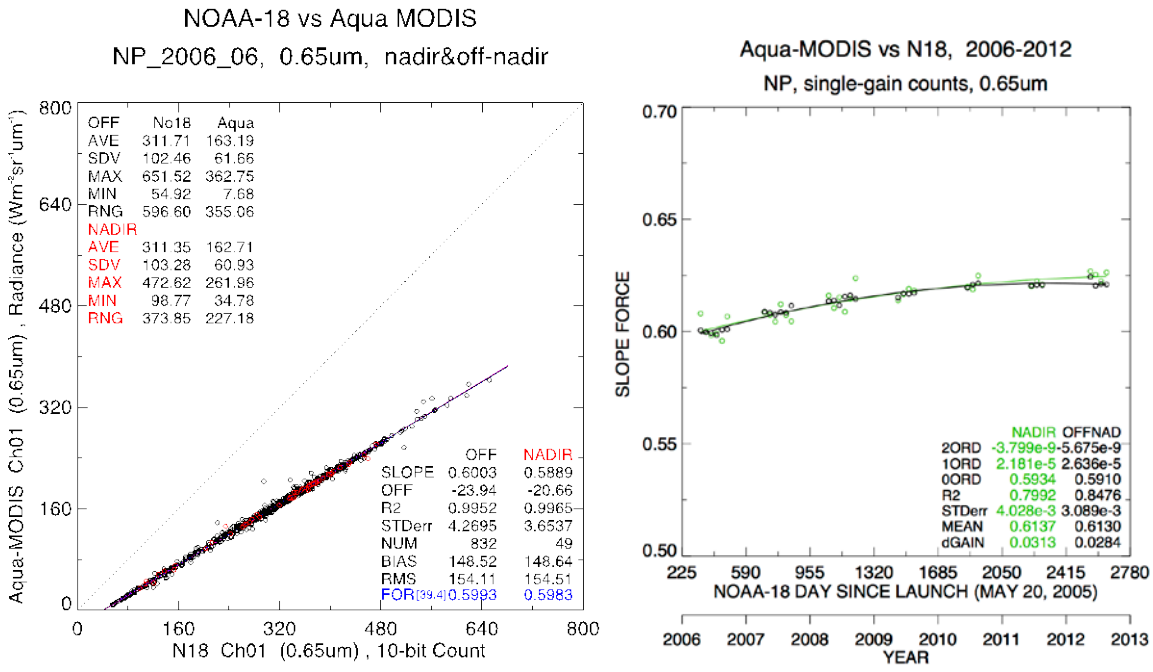

Figure 14: NOAA-18 AVHRR/Aqua-MODIS SNO VIS radiance pairs for June 2006. SNO trends computed from off-nadir (black) and nadir-only (green) monthly gains (left panel). Blue-labeled slopes in lower right corner represent linear regression through AVHRR VIS space count (slope force). Right panel displays the monthly slopes with associated trends.

3.4.2 Data Merging Strategy

To facilitate GOES/MODIS ray matching, both the GOES and MODIS gridded domain visible radiances, time, angles, locations are written out in single overpass or UTC image ASCII files. The program, which produces monthly satellite radiance pair plots, merges the two datasets by reading the two coincident ASCII files and identifying the matched angle and location for plotting. The monthly gains are saved in another file and the temporal plotting and regressing program reads from the monthly gain file.

The AVHRR/MODIS SNO does not grid on a fixed latitude-longitude grid, but locates 50-km diameter FOVs centered on the ground track intersection. Average FOV radiances are produced for each relevant channel for MODIS and AVHRR separately. The FOV mean channel radiances, times, angles, and locations for both satellites are written out in a single overpass ASCII file. The processing thereafter is similar to the GOES/MODIS procedures.

The SCIAMACHY and CERES SSF footprint data have been combined for the CLARREO project and the merged product is used to compute SBAFs. For a particular domain and scene type, the clear-sky Libya-4 desert for example, the SCIAMACHY/SSF footprint data are read in only to identify those footprints and write them to another domain/condition file. This facilitates processing of multiple satellite pairs.

After each AVHRR GAC or GOES area file is read, the invariant target instantaneous radiances are written out in single overpass or image files. These instantaneous files are combined to generate monthly files and read in by the program that computes the monthly desert and polar ice TOA radiances or DCC PDFs used to determine the monthly gains. The monthly gains are saved in a separate file. The temporal plotting and regression program reads data from this monthly gain file.

3.4.3 Numerical Strategy

Matlab and IDL statistic packages are used to determine regression statistics when needed, otherwise no numerical libraries are utilized.

3.4.4 Calculations

Navigation of the pixel data is effected using McIDAS GOES, NOAA AVHRR POD/KLM, and MODIS level1B (MYD03.A… files) routines. Simple statistics are used to grid pixel radiances. Pixel IRW temperatures and reflectances are first converted to radiances before averaging. Matlab, or IDL statistic packages or fortran90 code based on standard text books are used to determine regression statistics when needed.

The orbital prediction code used to determine the locations and time periods of ground track intersects is based on an in-house legacy code written prior to 1990. The orbital prediction code will not be provided, since there are plenty of web sites (http://www.ospo.noaa.gov/Products/ppp/navpage.html) and software, such as Analytical Graphics Incorporated (AGI) Satellite Toolkit (STK) and McIDAS, that can provide this information. The orbital prediction code generates ASCII files in which each line contains the ground track intersect latitude and longitude, and the crossing time and angles for each satellite and each crossing event. For AVHRR/MODIS SNO matching, only events with SZA < 70° are utilized. For GOES/MODIS matching, the orbital prediction program also predicts the number of regions within the GOES equatorial domain that are coincident and ray-matched. Events below a given threshold are not used in the analysis in order to save on computer resources.

3.4.5 Look-Up Table Description

The BRDF model developed by Hu et al. (2004) is used to remove the VZA and RAA dependencies of the DCC reflectances. The BRDF algorithm predicts the radiance as a function of SZA, VZA, and RAA.

3.4.6 Parameterization

None

3.4.7 Algorithm Output

The only FCDR data product produced is a netCDF file that contains the satellite specific calibration coefficients and uncertainty. It contains the AVHRR or GOES visible channel calibration gains as specified in Eq. 2., the space count as applied in Eq. 1, and the solar constant to convert the radiance into reflectance using Eq. 3. For AVHRR/3 the netCDF file contains the nominal intercepts, slopes and split count needed to convert the dual gain counts in to single gain counts using Eq. 6, 7, 8, 9. The file also contains the satellite names (TIROS-N, NOAA-6,…,Metop-A), the type of instrument (AVHRR/1, 2, or 3), the center wavelength of the visible bands, the launch date to compute the day since launch (DSL), the valid date range in both calendar and DSL units. Lastly, the calibration uncertainty is also included.

Similar for GOES the FCDF data product output is a netCDF file, except no nominal calibration parameters are included.

4. Test Datasets and Outputs

4.1 Test Input Datasets

Nor formal test datasets are provided.

4.2 Test Output Analysis

4.2.1 Reproducibility

The implementation of the calibration algorithm can be tested by reproducing the calibration coefficients provided in the FCDR.

4.2.2 Precision and Accuracy

See section 4.2.3.

4.2.3 Error Budget

4.2.3.1 Aqua-MODIS Absolute Calibration Uncertainty

The Aqua-MODIS band-1 0.65-µm absolute calibration uncertainty is from Xiong et al. (2005) and is 1.64% at launch. The Collection 6 temporal stability uncertainty is ~1% and may have darkened by 1% in later half of the Aqua record (Doelling et al. 2013). This version does not account for any temporal changes in the Aqua-MODIS VIS stability.

4.2.3.2 Incoming Solar Irradiance Uncertainty

The calibration of Aqua-MODIS is based on reflectance and the reflectances are converted to radiance using the MODIS official solar incoming irradiance. If the same incoming solar irradiance is used, whenever reflectances are required, then there is no uncertainty associated with the incoming irradiance. Doelling et al. (2009) convolved several solar incoming datasets with the GOES-11 SRF and found that the standard deviation of the resulting solar constants based on Equation 9 is 0.68%. This uncertainty is not factored into the overall calibration uncertainty.

4.2.3.3 SBAF Uncertainty

The SBAF or spectral band difference uncertainty is the slope uncertainty of the regression of the SCIAMACHY footprint pseudo radiance pairs. Since the invariant target and SNO/ray-matching methods produce monthly gains and therefor the mean atmospheric conditions, the SCIAMACHY footprint pseudo radiance pair slope uncertainty is considered rather than regression standard error. It is assumed that the conditions observed during the SCIAMACHY 9:30 LECT are also applicable to the AVHRR afternoon and morning orbit and Aqua sampling times. The SBAF computations yield ratios assume that SCIAMACHY has consistent relative spectral calibration, but does not necessarily require accurate absolute calibration.

Because the satellite pair SRFs usually overlap, it is assumed that the spectral calibration is consistent over the small range of wavelengths outside of either SRF. The absolute SCIAMACHY version-7.03 calibration uncertainty varies by band segment and can range from 2% in the red visible range up to 6% in the near infrared. No sensor SRF uncertainty is available; it is assumed that any degradation is uniform over the SRF.

4.2.3.4 Ray-Matching and SNO Calibration Uncertainty

The overall GEO/MODIS ray-matching or AVHRR/MODIS SNO uncertainty is the combination of the RM or SNO calibration transfer uncertainty and the associated SBAF uncertainty. The RM or SNO calibration transfer uncertainty is a direct transfer calibration approach, therefore, the uncertainty is based solely on the trend standard error of the monthly gains. It is assumed that the visible sensor degradation is gradual and monotonic. Given the seasonal cycle in the monthly gains, several years of monthly gains are needed to reduce the standard error. The confidence of trend detection is dependent on the natural variability of the measurements, the magnitude of the trend, and the length of the record (Weatherhead et al. 1998). The seasonal cycle is due to the movement of the brightest clouds, which follow the sun, and the associated angular matching conditions. For AVHRR, the SBAF uncertainty is the MODIS/NOAA-16 SBAF uncertainty over the northern polar domain. For GOES, the SBAF uncertainty is the MODIS/GOES-target over the GOES equatorial domain. Since the GEO imaging schedule repeats daily, the GEO/MODIS standard error maybe reduced by deseasonalization.

Only the nadir SNO locations can be used for most AVHRR platforms since they are in degrading orbits. If the satellites are maintained in a sun-synchronous orbit (e.g., MetOp), then off-nadir SNO locations may also be used to increase the monthly sampling and dynamic range significantly, which would reduce the overall uncertainty. Also, the monthly gains are limited to at 6 months out of the year. Near the terminator AVHRR may experience stray-light effects on the space count (Ignatov et al. 2005). The ray-matching and SNO uncertainty also relies on the stability of the Aqua-MODIS instrument. The SNO or ray-matching uncertainty therefor represents the lower bound. Since all methods reference the Aqua-MODIS calibration Collection 6 calibration it is not used in the overall uncertainty computation. Equation 15 describes how the SNO or ray-matching uncertainty is computed.

$$U_{SNO} = \sqrt{SNO^2 + SBAF^2_{SNO}} \qquad (15)$$

4.2.3.5 Desert and Polar Ice DM Uncertainty

The desert and polar ice DM uncertainty is the standard error of the DM regression and the associated SBAF uncertainty. For the specific case in Fig. 8 the regression standard error is 1.4%. For AVHRR, the SBAF uncertainty is the NOAA-16/NOAA-target SBAF uncertainty over the given Earth target. The DERM uncertainty is the standard deviation of the yearly TOA observations of the reference GEO satellite radiances averaged over all Julian days (for Fig. 10 right panel it is 1.2%). For GOES, the SBAF uncertainty is the GOES-reference/target SBAF uncertainty over the Sonoran desert.

4.2.3.6 DCC calibration DM Uncertainty

The DCC calibration transfer uncertainty is based on how well the GOES or AVHRR DCC mode radiance represents the Aqua-MODIS DCC mode radiance. The DCC methodology relies on accurately calibrated 11μm pixel level window IR BT to identify the DCC. The DCC reflectance is dependent on the DCC IRW temperature. An increase in the IRW BT threshold results in a smaller overall DCC reflectance (Doelling et al 2013). Mittaz et al. (2012) found for Metop-A the IRW temperatures were within 0.5K when compared with IASI. This translates into a 0.1% departure of the DCC mode reflectance, which was based on fact that decreasing the MODIS BTW by 5K resulted in a 0.5% increase in the DCC mode reflectance (Doelling et al. 2013).

For GOES, the transfer uncertainty is reduced by only considering DCC during the period of time when Aqua passes over the GOES domain. By ray-matching the GOES-13/Aqua-MODIS IRW BT pairs, it was found that the GOES-13 IRW BT difference was 1.5° at 205°K, which translated into calibration error of ~0.2% (Morstad et al. 2011). Only the GOES sensors operating during the MODIS era can be verified using this approach. It is assumed that the IRW calibrations are similar for all GOES-8 through 15, since GOES employs onboard blackbodies and space looks to maintain the calibration.

DCC calibration method does not require a DM for SZA < 40°. However in order to extend the DCC calibration method for SZA > 40° a DCC DM was derived. The DCC DM uncertainty then is the regression standard error of the DCC mode radiance as a function of μ0. Based on Fig. 12 the AVHRR DCC DM uncertainty is 0.76%. For GOES the DCC calibration method was not extended for SZA > 40° and therefor the DCC DM is not applicable.

4.2.3.7 Overall calibration error

The desert, polar ice, and DCC invariant target overall calibration uncertainty is the sum of the MODIS/NOAA-16 SNO with SBAF uncertainty, the invariant target DM with SBAF uncertainty, and the standard error (σ) about the temporal quadratic fit of the monthly gains. The desert method monthly gains are the combined desert gains described in section 3.4.1.6. Similarly, for the combined invariant target uncertainty, the standard error about the quadratic fit is from the monthly gains after desert, polar ice, and DCC monthly gains are combined according to section 3.4.1.6. This allows the method with the least variability about the trend to be the major contributor to the calibration, whereas the method with the greatest variability to have a much smaller contribution. The invariant DM uncertainty is also combined according to section 3.4.1.6. The DCC DM also includes the IRW uncertainty term. Since all methods reference the Aqua-MODIS calibration Collection 6 calibration it is not used in the overall uncertainty computation. Equation 15 shows how the combined invariant target uncertainty (U_{comb}) is computed.

$$U_{comb} = \sqrt{SNO^2_{withSBAF} + DM^2_{withSBAF} + \sigma^2} \qquad (16)$$

For GOES, the uncertainty does not include the polar ice method, since it is not used.

5. Practical Considerations

5.1 Numerical Computation Considerations

No numerical computational issues are considered. The processing speed is mainly limited by the I/O or the reading of the AVHRR, MODIS, SCIAMACHY/SSF and GOES daytime overpass files over the entire record as well as the input data file ingest from the NOAA CLASS and McIDAS servers. Data transfer time greatly exceeds that spent on computations. Once all of the radiance observations over the invariant targets and inter-calibration domains have been sequestered in an intermediate dataset, the analysis can be rerun quickly, since only ~1% of the original volume is needed.

5.2 Programming and Procedural Considerations

No optimization or parallel processing effort has been performed. CPUs with the fastest connectivity to the input disc are recommended to improve I/O speed.

5.3 Quality Assessment and Diagnostics

Sensor quality assessment is performed by visually examining the satellite trend plots for any monthly gain outliers for each of the calibration approaches. After the monthly outliers are identified, the instantaneous radiance pairs examined. Typically bad scan lines, erroneous navigation or time information can cause extreme outliers affecting the monthly gains. For AVHRR, the GAC files are occasionally corrupted after being downloaded from CLASS. In a similar manner, any outliers in the invariant target trend analysis are examined.

The NOAA17 AVHRR scan motor experienced instabilities starting January 10, 2010 and eventually stalled on October 15, 2010. Since September 28, 2010, the AVHRR data products have been deemed unusable due to increased degradation of the scan motor's performance.

The sensor quality is manifested in the trend standard error. The trend standard error increases with rising noise in the pixel counts or with any increased errors in the navigation and time observations. These changes will be recorded in the error budget.

5.4 Exception Handling

If the input quality flags or default values that indicate that the individual pixel or footprint data are not valid, they will not be utilized in the calibration approach. There is typically sufficient sampling over the invariant targets or matching domains for robust calibration computations.

5.5 Algorithm Validation

The GOES and AVHRR invariant target calibration approaches are evaluated by comparing them with the GOES/MODIS ray-matching or AVHRR/MODIS SNO calibration

during the MODIS era according to Table 1 and Table 2. During the pre-MODIS era, the invariant target calibrations are examined for consistency. For the AVHRR desert and polar ice invariant targets, the individual desert site monthly gains are visually examined for consistency. If a significant difference in the absolute calibration or a substantial temporal trend departure is observed, a review of the calibration algorithm is performed. If the gains from one or more of the desert or polar ice sites displays a drift not observed by the other targets during the sensor record, it is removed from the technique combination process. If the DCC invariant target reveals a trend not observed by the other invariant sites, then the temporal consistency of the sensor IRW BT is analyzed. In general, any inconsistencies among the calibration approaches are scrutinized.

5.6 Processing Environment and Resources

The processing is performed on many different platforms dependent on where the input data are located and what analysis is performed. The MODIS, AVHRR, and SCIAMACHY/SSF processing is performed on hardware at the NASA-LaRC ASDC, which utilizes a mixture of IBM Power6 and Power7+ and various Intel x86 processors totaling ~900 CPU cores. A two-petabyte online data storage requirement is met by employing IBM GPFS and storage systems. The GOES processing is performed on a Dell R510 platform utilizing x86 processors on 8 cores. Once the invariant target or SNO/ray-matching domain data has been written out as an intermediate data file, the analysis is performed on local MAC desktops. Programming languages include C, fortran90, and McIDAS fortran90/C to read the AVHRR, MODIS, GOES, and SCIAMACHY/SSF data utilizing HDF libraries. The temporal trend analysis is performed using Matlab, IDL and fortran90.

The AVHRR/MODIS SNO requires 600 GB of MODIS level 1B data and 15 GB of spatially sub-setted AVHRR GAC data from CLASS per satellite month. The DCC, desert, and polar ice calibrations require 5 GB, 0.4 GB, and 1.2 GB, respectively, of spatially sub-setted AVHRR GAC data from CLASS per satellite month. The GOES/MODIS ray-matching, DCC, and desert processing requires ~3GB per satellite month. The SCIAMACHY/SSF files total 1 GB per month.

The total download time from CLASS per satellite months for all AVHRR applications listed above is ~2.5 hours. These are uncompressed GAC files, since CLASS lacks a compression option before downloading. The time does not include the web ordering time. The GOES download and processing clock time using the McIDAS interface is ~1 hour per satellite month.

6. Assumptions and Limitations

6.1 Algorithm Performance

6.1.1 Invariant Target Stability

The invariant target calibration requires that the TOA reflectance is constant in time. Typically there are small seasonal fluctuations in TOA radiance over the invariant targets. It is assumed that these seasonal fluctuations are replicated annually. Employing long temporal records, seasonal SBAFs, and seasonal radiance models such as the DERM can help mitigate these fluctuations. Short-term fluctuations of the surface or cloud top reflectances are random and are typically initiated by rainfall (deserts), melting (polar ice), or variable convection microphysical (DCC) events. These events usually last a few months and do not impact the long-term calibration coefficients. Gradual long-term changes, which exceed the lifetime of a single satellite record are difficult to detect, and are assumed to be non-existent. Only the moon is a truly invariant target. All visible calibration methods ultimately rely on the sun for their stability, which varies by ~0.1% over an 11-year solar cycle.

6.1.2 Aqua-MODIS VIS Channel Lifetime Stability and Absolute Calibration

The SNO and RM methods transfer the Aqua-MODIS 0.65-μm calibration instantaneously. The invariant target radiance models utilize the Aqua-MODIS radiances collectively. Both approaches assume that the Aqua-MODIS calibration is stable over its lifetime. The Aqua-MODIS Collection 6 channel-1 lifetime stability is ~1% (Wu et al. 2013, Doelling et al. 2015).

The AVHRR and GOES calibrations rely on the absolute calibration of the Aqua-MODIS VIS band. The absolute Aqua-MODIS VIS calibration uncertainty is 1.64% based on errors in the ground to orbit calibration transfer. The natural variability of the invariant targets and current sensor calibration are limited in verifying the absolute calibration. In another decade, with the launch of CLARREO, the calibration uncertainty can be reevaluated.

6.1.3 Directional Models

The greatest challenge to AVHRR calibration is the degrading NOAA satellite orbits. The invariant target reflectance depends on the illumination angle, increasing with increasing solar zenith angles. Every effort is made to find the highest SZA threshold before these DMs are no longer useful. As the orbits degrade towards the terminator, the radiance signal-to-noise ratio is also reduced, due to increasing SZAs. Also taking advantage of the most isotropic of the angular configurations minimizes BRDF effects. Typically this occurs near nadir. Thus, data are used when the VZA < 10° for deserts and when VZA < 40° for DCC analyses.

6.2 Sensor Performance

6.2.1 AVHRR and GOES IRW brightness temperature

The DCC methodology relies on accurately calibrated IRW BTs to identify DCC pixels. An increase in the IRW temperature threshold typically results in a smaller DCC reflectance (Doelling et al 2013). If the observed temperature changes with respect to the true temperature, an artificial visible calibration drift will be manifested in the DCC calibration coefficients. If the IRW calibration is stable over time, but inaccurate, then the resulting DCC calibration will be artificially offset from the true calibration. The Aqua-MODIS DCC reference normalized radiance is assumed to be equivalent to the AVHRR/GOES sensor normalized radiance over the same domain and local time frame. This implies that the Aqua-MODIS band 31 10.8-µm and the AVHRR/GOES 10.8-µm temperatures are essentially equal.

It is assumed that the onboard blackbodies and space looks provide stable temperatures at 205°K during the lifetime of the satellite record. If the AVHRR/GOES sensor DCC calibration coefficients are similar to the SNO calibration during the MODIS era, the assumption is validated. Consistency between the desert and polar ice targets validates the DCC calibration during the pre-MODIS time frame.

6.2.2 AVHRR and GOES navigation

The FCDR relies on the nominal AVHRR and GOES navigation provided by the navigation elements accompanying the GAC and McIDAS files. All geo-referencing and solar and view angles are computed using the navigation elements. This may be a concern for desert and polar ice targets. The target region of interest domain is intentionally large (>50-km^2) in order to mitigate navigation shifts, since the surface reflectance may vary spatially. Similarly, the GEO/MODIS ray-matched radiance pairs are also on a 0.5°x0.5° lat/lon grid as are the AVHRR/MODIS SNO radiance pairs are from a 50-km^2 FOV. The large FOVs also reduce the misalignment of cloud features due to advection. Noisy detector, detector striping, or band co-registration errors will degrade the results of the DCC calibration (Bhatt et al. 2013).

The AVHRR GAC navigation errors are generally about 2 to 10-km (Heidinger et al 2010) and are probably similar for GOES. The MODIS navigation errors are on order of 150 m (Wolfe et al. 2006). The navigation accuracies of AVHRR and GOES are improving over time, with the greatest navigation uncertainty found for the earliest sensors. The navigation errors depend on the orbit characteristics and may be systematic.

6.2.3 Other sensor and orbit assumption and limitations

The visible sensor SRFs degradation is considered to be gray and not a function of wavelength. However, Decoster et al. (2013) provide evidence of wavelength-dependent degradation for wide band geostationary sensor SRFs.

The pre-launch SRFs are assumed to be correct for computing the sensor solar constant and SBAF. Some of the earlier SRFs also have low spectral resolutions (See ISCCP

SRFs http://isccp.giss.nasa.gov/response.html). The low resolution SRFs, may not capture all of the inflections in the true SRF, which can impact the SBAF if the unmeasured inflections are aligned with absorption spectra. It is assumed that the SCIAMACHY spectral radiances are properly calibrated in a relative sense, but are not necessarily absolutely calibrated.

Ignatov et al. (2005) report indications of small fluctuations in the visible AVHRR space count that are due to the heating and cooling of the spacecraft during each orbit, especially near the terminator. For this version, the AVHRR space count is assumed to be constant over time. This may impact dark clear-sky ocean radiances, which implies the potential for slight differences in the calibration gain over the equator when compared to polar conditions. Such variations highlight the need for more than one calibration approach to calibrate the suite of AVHRR and GOES sensors.

7. Future Enhancements

The following potential improvements will be tested for future versions.

7.1 Enhancement 1: AVHRR AM/PM SNOs

AVHRR sensor were flown in overlapping morning and afternoon orbits, permitting AVHRR AM/PM SNO radiance pairs to validate the relative calibration between coincident AVHRR AM and PM sensors. Doelling et al. (2001), Heidinger et al. (2002), and Heidinger et al. (2010) have employed AVHRR AM/PM SNO radiance pairs to transfer the calibration from one AVHRR sensor to another. For the visible channels the SNOs occur at ~80°N, where only the time period near the summer solstice provide SNOs with SZA < 70°. For the DCC calibration method consistent 205K IRW temperatures are required to maintain a consistent DCC albedo over the AVHRR record. Since the SNOs occur near the South pole, SNO temperature pairs near 205K can be compared.

7.2 Enhancement 2: GOES/MODIS DCC ray-matching

Currently GOES and Aqua-MODIS all-sky coincident radiance pairs over the tropics are regressed to obtain the monthly GOES calibration gain. Most of the radiance pairs are from clear-sky or dark targets. This is because it is difficult to fill a 0.5° latitude by 0.5° longitude region completely filled with bright clouds, which are needed to provide a the entire dynamic range of Earth reflected radiances. The dark targets also require strict angular constraints, since they are more anisotropic than bright clouds. Another ray-matching method will be developed that would only use deep convective radiance pairs. This has the advantage of ensuring bright radiance pairs to compute the calibration gain.

7.3 Enhancement 3: GOES South American desert target

For the GOES desert calibration approach, only the Sonoran desert is used. The desert calibration is then combined with the DCC calibration to provide the final historical GOES calibration coefficients. This contrasts with the AVHRR approach, which incorporates 4 desert, 2 polar ice targets, and DCC to derive the final calibration. The Sonoran desert site experiences short-term rain events (Angal et al. 2011). Multiple desert targets will increase the confidence of the GOES calibration. Several Atacama and Peruvian desert locations have been analyzed for stability. These desert sites are not as useful as the Sonoran, since they are cloudy during a few months over the year. However, when they are cloud free they provide stable TOA radiances. The incorporation of these sites will increase the confidence of the historical calibration of GOES sensors.

7.4 Enhancement 4: Historical GOES space counts

It was found for GOES-5 through 7 that the space count based on unlit disc can vary over time, especially for GOES-7. This is in part due to the ISCCP B1U processing agency (Inamdar and Knapp 2105). Also, the historical GOES imagers did not employ detector equalization algorithms at the satellite level (Frouin and Simpson 1995). This may result in a large variance of the space count.

8. References

Angal, A., G. Chander, X. Xiong, T. Choi, and A. Wu (2011), Characterization of the Sonoran desert as a radiometric calibration target for Earth observing sensors. *J. Appl. Remote Sens.*, 5, 059502.

Barnes, W. L., T. S. Pagano, and V. V. Salomonson (1998), Prelaunch characteristics of the moderate resolution imaging spectroradiometer (MODIS) on EOS-AM1. *IEEE Trans. Geosci. Remote Sens.*, 36, 1088–1100.

Bhatt, R., D. R. Doelling, D. L. Morstad, B. R. Scarino, and A. Gopalan (2013), Desert-based absolute calibration of successive geostationary visible sensors using a daily TOA radiance model. *IEEE Trans. Geosci. Remote Sens.*, TGRS-2012-00253, in press.

Bhatt, R., D. R. Doelling, B. R. Scarino, A. Gopalan, and C. O. Haney (2013), An initial assessment of the VIIRS onboard calibration using DCC and desert referenced to the Aqua-MODIS calibration. *Proc. 2013 SPIE Optics and Photonics*, San Diego, CA, August 25-29.

Bhatt, R., D. R. Doelling , A. Wu, X. Xiong, B. R. Scarino, C. O'Haney, and A. Gopalan (2013), Initial calibration stability assessment of S-NPP VIIRS reflective solar bands using invariant desert and deep convective cloud targets. *Remote Sens.*, submitted.

Bovensmann, H., J. P. Burrows, M. Buchwitz, J. Frerick, S. Noël, V. V. Rozanov, K. V. Chance, and A. P. H. Goedec (1999), SCIAMACHY: Mission objectives and measurement modes, *J. Atmos. Sci.*, 56, 127–150.

Clark, J. D. (1983), The GOES User's Guide. (http://www.ncdc.noaa.gov/oa/documentlibrary/GOES_Users_Guide_1983.pdf)

Decoster, I, N. Clerbaux, E. Baudrez, S. Dewitte, A. Ipe, S. Nevens, A. Velazquez Blazquez, and J. Cornelis (2013), A spectral aging model for the *Meteosat-7* Visible Band*, J. Atmos. Oceanic Technol.,* 30, 496-509*,* doi: http://dx.doi.org/10.1175/JTECH-D-12-00124.1.

Doelling, D. R., V. Chakrapani, P. Minnis, L. Nguyen (2001), The calibration of NOAA-AVHRR visible radiances with VIRS. Proc. AMS 11th Conf. Atmos. Radiation, Madison, WI, Oct 15–18, 614-617, 2001.

Doelling, D.R., L. Nguyen, and P. Minnis (2004), On the use of deep convective clouds to calibrate AVHRR data. *Proc. SPIE*, 5542, doi: 10.1117/12.560047.

Doelling, D., D. Morstad, R. Bhatt, and B. Scarino (2011), Algorithm Theoretical Basis Document (ATBD) for Deep Convective Cloud (DCC) technique of calibrating GEO sensors with Aqua-MODIS for GSICS. 11 pp. Available at https://gsics.nesdis.noaa.gov/wiki/Development/AtbdCentral\

Doelling, D., R. Bhatt, D. Morstad, and B. Scarino (2011), Algorithm Theoretical Basis Document (ATBD) for ray-matching technique of calibrating GEO sensors with Aqua-MODIS for GSICS, 10 pp. Available at https://gsics.nesdis.noaa.gov/wiki/Development/AtbdCentral\

Doelling, D. R., C. Lukashin, P. Minnis, B. Scarino, and D. Morstad (2012), Spectral reflectance corrections for satellite intercalibrations using SCIAMACHY data. *IEEE Geosci. Remote Sens. Lett.*, 9, 119-123 (2012).

Doelling, D. R., B. R. Scarino, D. Morstad, A. Gopalan, R. Bhatt, C. Lukashin, and P. Minnis (2013), The intercalibration of geostationary visible imagers using operational hyperspectral SCIAMACHY radiances. *IEEE Trans. Geosci. Remote Sens.*, 51, 1245-1254.

Doelling, D. R., D. Morstad, B. R. Scarino, R. Bhatt, and A. Gopalan (2013), The characterization of deep convective clouds as an invariant calibration target and as a visible calibration technique. *IEEE Trans. Geosci. Remote Sens.*, 51, 1147-1159, doi: 10.1109/TGRS.2012.2225066.

Doelling, D.R., A. Wu, X. Xiong, B.R. Scarino, R. Bhatt, C.O. Haney, D. Morstad, A. Gopalan (2015), The radiometric stability and scaling of collection 6 Terra and Aqua-MODIS VIS, NIR, and SWIR spectral bands. IEEE Trans. Geosci. Remote Sens., Vol. 53, No. 8, 4520-4535, DOI: 10.1109/TGRS.2015.2400928

Frouin, R., and J. J. Simpson (1995), Radiometric calibration of GOES-7 VISSR solar channels during the GOES Pathfinder benchmark period. *Remote Sens. Environ.,* 52, 95-115

Goldberg, M., G. Ohring, J. Butler, C. Cao, R. Datla, D. Doelling, V. Gärtner, T. Hewison, B. Iacovazzi, D. Kim, T. Kurino, J. Lafeuille, P. Minnis, D. Renaut, J. Schmetz, D. Tobin, L. Wang, F. Weng, X. Wu, F. Yu, P. Zhang, and T. Zhu (2011), The Global Space-based Inter-Calibration System (GSICS). *Bull. Am. Meteorol. Soc.*, 92, 467-475.

Heidinger, A. K., C. Cao, and J. T. Sullivan (2002), Using Moderate Resolution Imaging Spectrometer (MODIS) to calibrate advanced very high resolution radiometer reflectance channels. *J. Geophys. Res.*, 107, doi:10.1029/2001JD002035.

Heidinger, A. K., W. C. Straka III, C. C. Molling, J. T. Sullivan, and X. Wu, (2010). Deriving an intersensor consistent calibration for the AVHRR solar reflectance data record. *International J. Remote Sens,* 31, 6493-6517.

Hu, B, B. A. Wielicki, P. Yang, P. W. Stackhouse, Jr., B. Lin, and D. F. Young (2004), Application of deep convective cloud albedo observation to satellite-based study of the terrestrial atmosphere: Monitoring the stability of spaceborne measurements and assessing absorption anomaly. *IEEE Trans. Geosci. Remote Sens.*, 42, 2594–2599.

Ignatov, A., C. Cao, J. Sullivan, R. Levin, X. Wu, and R. Galvin (2005), The usefulness of in-flight measurements of space count to improve calibration of the AVHRR solar reflectance bands. *J. Atmos. Oceanic Technol.,* 22, 180-200.

Inamdar, A.K., K. R. Knapp (2015), Intercomparison of Independent Calibration Techniques Applied to the Visible Channel of the ISCCP B1 Data, . *J. Atmos. Oceanic Technol.,* 32, 1225-1240, DOI: 10.1175/JTECH-D-14-00040.1

Lazzara, M. A., and Coauthors (1999), The Man computer Interactive Data Access System: 25 years of interactive processing. *Bull. Amer. Meteor. Soc.*, 80, 271–284.

Menzel, W. P. and J. F. W. Purdom (1994), Introducing GOES-I: The first of a new generation of Geostationary Operational Environmental Satellites. *Bull. Amer. Meteor. Soc.*, 75, 757–781.

Minnis, P. (2014), A consistent long-term cloud and clear-sky radiation property dataset from the Advanced Very High Resolution Radiometer (AVHRR) Climate Algorithm Theoretical Basis Document (C-ATBD). *NOAA C-ATBD DSR-XXX*, available at NCDC.

Minnis, P., L. Nguyen, D. R. Doelling, D. F. Young, W. F. Miller, and D. P. Kratz (2002), Rapid calibration of operational and research meteorological satellite imagers, Part I: Evaluation of research satellite visible channels as references. *J. Atmos. Oceanic Technol.*, 19, 1233-1249.

Minnis, P., D. R. Doelling, L. Nguyen, W. F. Miller, and V. Chakrapani (2008), Assessment of the visible channel calibrations of the TRMM VIRS and MODIS on *Aqua* and *Terra*. *J. Atmos. Oceanic Technol*., 25, 385-400.

Minnis, P., S. Sun-Mack, D. F. Young, P. W. Heck, D. P. Garber, Y. Chen, D. A. Spangenberg, R. F. Arduini, Q. Z. Trepte, W. L. Smith, Jr., J. K. Ayers, S. C. Gibson, W. F. Miller, V. Chakrapani, Y. Takano, K.-N. Liou, Y. Xie, and P. Yang (2011), CERES Edition-2 cloud property retrievals using TRMM VIRS and Terra and Aqua MODIS data, Part I: Algorithms. *IEEE Trans. Geosci. Remote Sens.*, 49, 4374-4400.

Mittaz, J., and A Harris, 2011: A Physical Method for the Calibration of the AVHRR/3 Thermal IR Channels. Part II: An In-Orbit Comparison of the AVHRR Longwave Thermal IR Channels on board MetOp-A with IASI, *J. Atmos. Oceanic Technol.*, 28, 1072-1087, DOI: 10.1175/2011JTECHA1517.1

Morstad, D. L., D. R. Doelling, R. Bhatt, and B. Scarino (2011), The CERES calibration strategy of the geostationary visible channels for CERES cloud and flux products. *Proc. SPIE Earth Observing Systems XVI*, 8153, 815316, September 13.

Scarino, B., D. R. Doelling, D. L. Morstad, R. Bhatt, A. Gopalan, C. Lukashin, and P. Minnis (2012), Using SCIAMACHY to improve corrections for spectral band differences when transferring calibration between visible sensors. *Proc. Earth Observing Systems XVII*, Proc. SPIE, 8510, 85100Q, October 15, doi:10.1117/12.929767.

Scarino, B.R., D.R. Doelling, P. Minnis, A. Gopalan, T. Chee, R. Bhatt, C. Lukashin, C. Haney (2015), A Web-based Tool for Calculating Spectral Band Difference Adjustment Factors

Derived from SCIAMACHY Hyper-spectral Data, *IEEE Trans. on Geosci. Remote Sen.*, submitted.

Weatherhead, E. C., and Coauthors (1998), Factors affecting the detection of trends: Statistical considerations and applications to environmental data. J. Geophys. Res., 103 (D14), 17 149–17 161.

Weinreb, M., M. Jamieson, N. Fulton, Y. Chen, J. X. Johnson, J. Bremer, C. Smith, and J. Baucom (1997), Operational calibration of Geostationary Operational Environmental Satellite-8 and -9 imagers and sounders, *Applied Optics*, Vol. 36, No. 27, 6895-6904

Wolfe, R. E., M. Nishihama, A. J. Fleig, J. A. Kuyper, D. P. Roy, J. C. Storey, and F. S. Patt (2002), Achieving sub-pixel geolocation accuracy in support of MODIS land science. *Remote Sens. Environ.*, 83, 31-49.

Wu, A., Xiong, X., Doelling, D. R., Morstad, D. L., Angal, A., and Bhatt, R. (2013), Characterization of Terra and Aqua MODIS VIS, NIR, and SWIR spectral band calibration stability. *IEEE Trans. on Geosci. Remote Sen.*, 10.1109/TGRS.2012.2226588.

Xiong, X., J. Sun, A. Wu, K. Chiang, J. Esposito, and W. Barnes (2005), Terra and Aqua MODIS calibration algorithms and uncertainty analysis. *Proc. Sensors, Systems, and Next-Generation Satellites IX*, Proc. SPIE Vol. 5978, 59780V, doi:10.1117/12.627631.

Yu, F. and X. Wu (2010), Water vapor correction to improve the operational calibration for NOAA AVHRR/3 channel 2 (0.85 μm) over a desert target. *Can. J. Remote Sens.*, 36, 514–526.

Appendix A. Acronyms and Abbreviations

Acronym or Abbreviation	Meaning
ASDC	Atmospheric Science Data Center
AVHRR	Advanced Very High Resolution Radiometer
BRDF	Bidirectional Reflectance Distribution Function
BT	Brightness Temperature
C-ATBD	Climate Algorithm Theoretical Basis Document
CDR	Climate Data Record
CERES	Clouds and the Earth's Radiant Energy System
CLARREO	Climate Absolute Radiance and Refractory Observatory
CLASS	Comprehensive Large Array-data Stewardship System
DERM	Daily Exoatmospheric Radiance Model
DCC	Deep Convective Cloud
DM	Directional Model
FCDR	Fundamental Climate Data Record
FOV	Field Of View
GAC	Global Area Coverage
GOES	Geostationary Operational Environmental Satellite
GSICS	Global Space-based Inter-Calibration System
HRPT	High Resolution Picture Transmission
IASI	Infrared Atmospheric Sounding Interferometer
IJPS	International Joint POES System
IRW	Infrared Window (10.8 μm)
LAC	Local Area Coverage
LaRC	Langley Research Center
LECT	Local Equator Crossing Time
LUT	Look Up Table
McIDAS	Man-computer Interactive Data Access System
MCST	MODIS Characterization Science Team
MetOp	Meteorological Operational Polar Satellite
MODIS	MODerate-resolution Imaging Spectrometer
NASA	National Aeronautics and Space Administration

NIR	Near InfraRed (1.6 μm)
NCDC	National Climate Data Center
Acronym or Abbreviation	**Meaning**
NOAA	National Oceanographic and Atmospheric Administration
NORAD	North American Aerospace Defense
PATMOS-X	Pathfinder Atmospheres Extended
PDF	Probability Distribution Function
POD	Polar Orbiter Data
POES	Polar Orbiting Environmental Satellite
RAA	Relative Azimuth Angle
RM	Ray-Matching
ROI	Region Of Interest
SBAF	Spectral Band Adjustment Factor
SCIAMACHY	SCanning Imaging Absorption spectroMeter for Atmospheric CartograpHY
SIR	Shortwave InfraRed (~3.75 μm)
SIST	Shortwave-infrared Infrared Split-window Technique
SNO	Simultaneous Nadir Overpass
SRF	Spectral Response Function
SSF	Single Scanner Footprint
SWI	Split Window Infrared (~12.0 μm)
SZA	Solar Zenith Angle
TCDR	Thematic Climate Data Record
TLEs	Two-Line Element sets
UTC	Universal Coordinated Time
VEG	Vegetation Channel (~0.86 μm)
VIS	Visible (~0.64 μm)
VISSR	Visible Infrared Spin Scan Radiometer
VZA	Viewing Zenith Angle